Peertechz

Journal of
Cardiovascular Medicine and Cardiology
OPEN ACCESS JOURNAL

ISSN: 2455-2976 Journal DOI: https://dx.doi.org/10.17352/jcmc

Research Article

On the Heart Rhythm Analysis by an Intelligent Control Method Using Artificial Neural Networks: Analytical Study and Electronic Simulation

RF Fonkou[1]*, Gabriel S Lima[2] and Marcelo A Savi[3]

[1]Research Unit Condensed Matter, Electronics and Signal Processing, University of Dschang, P.O. Box 67 Dschang, Cameroon

[2]Programa de Pós-Graduação em Engenharia Elétrica e de Computação, Universidade Federal do Rio Grande do Norte, Natal, Brazil

[3]Department of Mechanical Engineering, Universidade Federal do Rio de Janeiro, Rio de Janeiro, Brazil

Submitted : 25 May, 2026
Accepted : 24 June, 2026
Published : 25 June, 2026

***Corresponding author:** RF Fonkou, Research Unit Condensed Matter, Electronics and Signal Processing, University of Dschang, P.O. Box 67 Dschang, Cameroon, Email: fonkourodrigue99@yahoo.com

Keywords: Electrocardiogram (ECG) signal; Analysis of stability; Ntelligent control method; Duffing-type connections; Feedback linearization method (FBL); Artificial neural network; OrCAD-Pspice

https://www.organscigroup.com

Check for updates

Abstract

One of the fundamental characteristics of the Heart's physiology is its heart rate. Heart rhythms are interpreted by Electrocardiogram (ECG) signals, which enable a better analysis of normal and pathological rhythms. For its normal functioning, the heart is modeled as an electrical system that generates its own electricity, and which enables to beat and play its role as a pump. This system is called the electrical conduction system of the heart. The electricity generated by the heart ensures contraction of the atria and ventricles. In this work, an intelligent control method is presented to establish a test for heart rhythm control, and the implementation of an electronic circuit for the heart model used is carried out. For a better analysis of the model used, an analysis of stability in its autonomous, unidirectionally coupled state is carried out. It reveals regions of stable and unstable periodicities describing very rich dynamic behaviours. The sinus node being the initiator of the electrical current that powers the heart, a control strategy for tracking sinus node signal trajectories in the event of a disturbance is developed. The observed dynamic is the Electrocardiogram (ECG) signal. To generate it, the heart is modeled on a network of three nonlinear oscillators linked by delayed Duffing-type connections: the sinus node, the atrioventricular node and the Purkinje His bundle. Other specificities of the cardiac rhythm are linked by external stimuli. The controlled variable is the sinus node signal. For better compensation of unknown or hidden heart dynamics, digitally, the feedback linearization method (FBL) by integrating an artificial neural network to compensate for the unknown dynamics is used. Based on synthetic ECGs, the results obtained show that FBL enables the heart to maintain its normal rhythm, avoiding pathological rhythms. For real-life implementation, an electronic simulation using analog components from OrCAD-Pspice software is carried out. The results obtained are in qualitative agreement.

Introduction

The regular and normal pumping of blood by the biological organs conditions the normal functioning of the heart [1-5]. Knowledge of cardiac activity is crucial in the analysis of the heart, as it can be regular or irregular in time and space [6,7]. Under certain conditions, this regularity or irregularity can reveal pathologies [8, 9]. These pathologies are identified by analysis of the cardiac system. The cardiac electrical system maintains its rhythm between 60 and 100 beats per minute. The functional diagram of the heart, with its main cardiac nodes representing the cardiac electrical conduction system, is shown in figure 1a. The normal response of a normal ECG, consisting of the main waves: the P wave, the QRS complex and the T wave, is shown in figure 1b.

The cardiac system is made up of nodes ranging from the SA node, the AV node to the Purkinje fibers [12-15]. It functions like a pacemaker, so the precise point of electrical current creation is the sinus node, located at the apex of the right atrium. The electrical

Citation: Fonkou RF, Lima GS, Savi MA. On the Heart Rhythm Analysis by an Intelligent Control Method Using Artificial Neural Networks: Analytical Study and Electronic Simulation. J Cardiovasc Med Cardiol. 2026;13(3):42-72. Available from: https://dx.doi.org/10.17352/2455-2976.000242

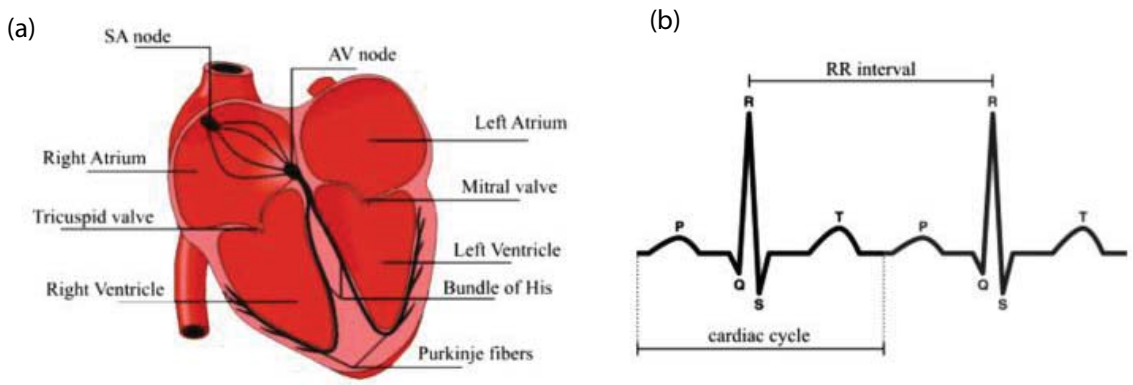

Figure 1: Functional diagram of the electric system of conduction of the heart [10,11].

current is a few millivolts and is generated from a cluster of cells. From the sinus node, the current spreads like an oil slick through the heart muscle. It flows through the 2 atria to their base, causing them to contract. Then, through an electrical relay called the Atrioventricular Node (AVN), the electric current reaches the septum separating the atria and ventricles. Each electrical current path between the sinoatrial node and the ventricles causes a heartbeat. This sequence of electrical current flow from the sinus node to the Purkinje fibers is the origin of the electrocardiogram signal. The electrocardiogram records a succession of sequences of the heart's electrical activity, represented by P waves, the QRS complex and the T wave. The P wave is that of the atria at the moment of their contraction, the QRS complex corresponds to the contraction of the ventricles, and the T wave reflects the repolarization (return to the resting phase) of the ventricles. When the formation or conduction of electrical excitation is disrupted, we speak of arrhythmias [16-21].

In 1928, Van der Pol and Van der Mark proposed the first nonlinear oscillator model capable of modeling the pacemaker [22]. This oscillator is considered the starting point for cardiac modeling. Still with the aim of modeling heartbeats, a large number of pacemaker models have been proposed as nonlinear oscillators like Van der Pol. We note the works of Fonkou et al [23-27], FitzHugh [28] and Hodgkin-Huxley [29]. These oscillators present important characteristics, in particular their ability to undergo frequency entrainment phenomenon without altering their amplitudes, since the main pacemaker is the element of the conducting system with the highest frequency, to which all the other oscillators must adapt.

It should be noted that the study of the cardiac conduction system at the cellular level is not suited to this approach to heartbeat modeling, as it only enables an analysis of the heart rhythm to be made by studying the interactions between the various elements. In this option, based mainly on the interactions between cardiac nodes, numerous works have been done focusing mainly on the interaction between AV, SA nodes and Purkinje His bundles. Among these works, we note in 2009 the work of Gois and Savi [30]. They model the cardiac system as a set of three Grudzinski-Zebrowski oscillators coupled unidirectionally to each other by delayed connections. In 2022, Fonkou et al [31] also proposed a model of the heart as an ensemble of three FitzHugh-Nagumo-type oscillators coupled by delayed connections. In 2021, Cheffer et al improved on the model proposed by Gois and Savi [32]. In the same context, random connections have been studied [33-35]. In 2023 Fonkou and Savi improved the heart system by proposing a reduced-order model to describe different heart rhythms by incorporating delayed Duffing-type connections. They also described variations in sinus rhythm by a time-dependent frequency, representing transient disturbances [36]. We also note the work of Krstacic et al [37], Ernst and Bar-Joseph [38], Tobon et al [39].

However, a large number of external and physiological constraints can affect cardiac activity, leading to the appearance of life-threatening pathologies requiring a controller in these situations. Among these controllers we can mention artificial pacemakers and implantable heart defibrillators. The latter are devices capable of impacting heart rhythm management, as they are for the most part powered by batteries that need to be replaced or recharged after a period of operation. They must therefore be monitored by appropriate controllers linked to probes that monitor heart activity or body response [40]. In recent years, the concept of monitoring has emerged as a plausible way of optimizing and automating biological assist devices, including artificial pacemakers [40,41].

In this context, a large number of approaches to heart rate control have been developed [42-44]. These include the classic method of Garfinkel et al [42, 45], and the work of Ferreira et al [46], in which they control the dynamics of a pacemaker using feedback control. In 2014, they proposed a more general analysis for ECG control [47], which stabilizes unstable periodic orbits embedded in chaotic attractors allowing critical physiological situations to be managed. In 2020, Lounis et al [44] developed a highorder control method to solve the dynamic problems of the model proposed by Quiroz-Juarez et al [48]. In 2020, an active control based on the Lyapunov method was proposed by Khan and Nigar [49]. Faced with the difficulty of solving all the non-linearity problems inherent in systems, such as approximation errors and external disturbances, some control methods appear to be ineffective. Some researchers

Citation: Fonkou RF, Lima GS, Savi MA. On the Heart Rhythm Analysis by an Intelligent Control Method Using Artificial Neural Networks: Analytical Study and Electronic Simulation. J Cardiovasc Med Cardiol. 2026;13(3):42-72. Available from: https://dx.doi.org/10.17352/2455-2976.000242

have tried to solve them using the state observer method [50]. This method has not been satisfactory because it is limited. Others, however, have used machine learning incorporating artificial neural networks (ANNs) [51-53]. This method has proved highly effective. For example, in 2023, Lima et al., [41] developed an intelligent control method using artificial neural networks to eliminate heart rhythm problems. In their work, they evaluate the ability of the control law to manage intra- and inter-patient variability by considering the control variable at the level of the His-Purkinje complex. Machine learning, for its part, may offer attractive options for dealing with this. Artificial neural networks (ANNs), for example, have been used to identify and classify heart rhythm diseases [51-53]. Because of their learning and approximation capabilities, neural networks have also been used in control applications to compensate for model uncertainties and perturbations [54-57].

In this article, considering the reduced-order model developed by Fonkou and Savi [36], consisting of three non-linear oscillators linked by delayed Duffing-type connections, a test for the control of heart rhythm is carried out. In order to have an overall idea of the behavior of the model, an analysis of its stability in its autonomous, unidirectionally coupled state is carried out. It reveals regions of stable and unstable periodicities describing very rich dynamic behaviors. Since the electrical signal responsible for powering the heart's organs is generated by the SA node, a disturbance of the heart rhythm is caused at the SA node, leading to the appearance of cardiac pathologies such as ventricular fibrillation, ventricular flutter, atrial fibrillation and atrial flutter. To manage this, a control strategy has been developed. It consists in following the signal trajectories of the sinus node. For better compensation of unknown or hidden heart dynamics, the feedback linearization method (FBL) is used numerically, integrating Artificial Neural Networks (ANNs) to compensate for unknown dynamics. The observed dynamic is the electrocardiogram (ECG) signal. Based on synthetic ECGs, the results obtained show that FBL enables the heart to maintain its normal rhythm, avoiding pathological rhythms. In order to also achieve a real-life implementation of the model used, an electronic simulation of the heart system was carried out using OrCAD-PSpice software. The results obtained show good agreement with those obtained numerically.

The rest of the work is organized as follows: the mathematical modeling of the heart model is presented in section 2. System stability is analyzed in session 3. It shows regions of stable and unstable periodicities describing very rich dynamics. Section 4 presents the normal dynamics of the synthetic ECG. Pathological ECGs are highlighted in section 5. The details of the controller are developed in section 6. Section 7 shows the impact of control on the system. Results obtained by electronic simulation on OrCAD-PSpice are given in section 8. The work ends with a conclusion in section 9.

Mathematical modelling

As is well known, two pumps - the left and right ventricles - are essential parts of the heart. They are contracted by the electrical impulse produced by the heart through its electrical system, known as the electrical conduction system of the heart. Its role is to ensure a regular heartbeat. For good functioning of the electrical conduction system, the amount of blood needed to oxygenate the lungs is pumped by the right ventricle, and the amount of blood needed to oxygenate the whole body is pumped by the left ventricle. This analysis shows that the greatest mechanical work is done by the left ventricle. All this is due to the regularity of the cardiac conduction system It is composed of the sinus node, the atrioventricular node and Purkinje's His bundles. The electrical impulse which causes the contraction of the atria and ventricles is initiated by the sinus node (the heart's natural pacemaker). After receiving information from the brain, the SA node adapts the heart rate in accordance with the body's energy requirements. In its normal state, heart rate varies between 1 and 1.67 Hz. The electrical impulse initiated by the SA node enables the blood to reach the ventricles after having passed through the two auricles by contracting them. The atrioventricular node in turn receives this electricity, filters it, slowing it down, if necessary, in cases of rhythm disorders, and then directs it through Purkinje's His bundles to the ventricles, also enabling the ventricles to contract. This is how electricity travels through the heart. Each heartbeat forming the electrocardiogram (ECG) signal is caused by each electrical current pathway from the sinus node to the ventricles.

Recent work has shown that heartbeat modeling is a crucial process for the automatic identification of characteristic waves [10,11]. The objective is to propose the simplest, most compact mathematical model capable of qualitatively and quantitatively simulating the shape of the five main waves (P,Q,R,S and T waves) constitutive of heartbeats. Indeed, the most natural representation of the waves would be to describe the signal by its amplitude at each instant; this representation would therefore be a vector in a space whose dimension would be equal to a few hundred. From these analyses, cardiac physiology has been modeled as a system of three oscillators subjected to external stimuli and coupled together by delayed connections [36]. These stimuli have the effect of increasing the dimension of the reduced-order model system and also represent spatio-temporal stimuli.

In this subsection, the mathematical model is that proposed by Fonkou and Savi [36]. This is a system of three nonlinear oscillators coupled by delayed Duffing-type connections incorporating cubic non-linear terms. These three oscillators consist of the SA node, the AV node and the Purkinje fibers linked by Duffing-type connections with delay and non-delay. For this work, in addition to the external stimuli to which each oscillator is subjected, the SA oscillator is subjected to the controller u as presented by its conceptual model of general functioning given in figure 2. The mathematical model describing them is given by equation (1).

Citation: Fonkou RF, Lima GS, Savi MA. On the Heart Rhythm Analysis by an Intelligent Control Method Using Artificial Neural Networks: Analytical Study and Electronic Simulation. J Cardiovasc Med Cardiol. 2026;13(3):42-72. Available from: https://dx.doi.org/10.17352/2455-2976.000242

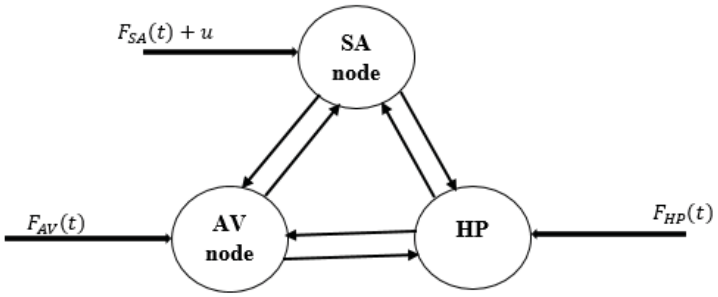

Figure 2: Conceptual model of general functioning of the heart with controller.

$$
\begin{aligned}
\dot{x}_1 &= x_2 \\
\dot{x}_2 &= F_{SA}(t) - \alpha_{SA} x_2 \left(x_1 - v_{SA_1}\right)\left(x_2 - v_{SA_1}\right) - \omega \frac{x_1\left(x_1 - d_{SA}\right)\left(x_1 - e_{SA}\right)}{d_{SA} e_{SA}} - k_{AV-SA}\left(x_1 - x_1^3\right) - k_{HP-SA}\left(x_1 - x_1^3\right) \\
&\quad + k^{\tau}_{AV-SA}\left(x_3^{\tau AV-SA} + \left(x_3^{\tau AV-SA}\right)^3\right) + k^{\tau}_{HP-SA}\left(x_5^{\tau HP-SA} + \left(x_5^{\tau HP-SA}\right)^3\right) + u \\
\dot{x}_3 &= x_4 \\
\dot{x}_4 &= F_{AV}(t) - \alpha_{AV} x_4 \left(x_3 - v_{AV_1}\right)\left(x_3 - v_{AV_1}\right) - \frac{x_3\left(x_3 + d_{AV}\right)\left(x_3 + e_{AV}\right)}{d_{AV} e_{AV}} - k_{SA-AV}\left(x_3 - x_3^3\right) - k_{HP-AV}\left(x_3 - x_3^3\right) \\
&\quad + k^{\tau}_{SA-AV}\left(x_1^{\tau SA-AV} + \left(x_1^{\tau SA-AV}\right)^3\right) + k^{\tau}_{HP-SA}\left(x_5^{\tau HP-AV} + \left(x_5^{\tau HP-AV}\right)^3\right) \\
\dot{x}_5 &= x_6 \\
\dot{x}_6 &= F_{HP}(t) - \alpha_{HP} x_6 \left(x_5 - v_{HP_1}\right)\left(x_5 - v_{HP_1}\right) - \frac{x_5\left(x_5 - d_{HP}\right)\left(x_5 - e_{HP}\right)}{d_{HP} e_{HP}} - k_{SA-HP}\left(x_5 - x_5^3\right) - k_{AV-HP}\left(x_5 - x_5^3\right) \\
&\quad + k^{\tau}_{SA-HP}\left(x_1^{\tau SA-HP} + \left(x_1^{\tau SA-HP}\right)^3\right) + k^{\tau}_{AV-HP}\left(x_3^{\tau AV-HP} + \left(x_3^{\tau AV-HP}\right)^3\right)
\end{aligned}
\tag{1}
$$

Where u is the controller. The SA, AV and HP nodes are described respectively by the pairs $(x_1, x_2), (x_3, x_4)$ *and* (x_5, x_6). Coefficients between two nodes m and $n (m \neq n)$ without delay and with delay are given by k_{m-n} and k^{τ}_{m-n} (m and n can express the SA, AV or HP node as well). The linear and cubic terms with delay are: $x_j^{\tau m-n} = x_j\left(t - \tau_{m-n}\right)$ and $\left(x_j^{\tau m-n}\right)^3 = \left(x_j\left(t - \tau_{m-n}\right)\right)^3$, and those without delay are x_j and ${x_j}^3 (j = 1, 2, \ldots, 6). F_n(t) = \rho_n \sin\left(\omega_n t\right)$ is the external excitation making the system temporarily dependent and increasing its dimension. ω is the transient frequency disturbing the SA node. It is a function of time and is described by

$$
\omega = \omega(t) = \frac{\omega_a + \omega_b}{2} + \frac{\omega_a - \omega_b}{2} tanh\left[\gamma\left(t - t_0\right)\right] \tag{2}
$$

$\frac{\omega_a - \omega_b}{2}$ is the transitional phase between ω_a and ω_b, t_0 the transition time. In this work its influence will be neglected, it will take the values $\omega_a = \omega_b = 1$

Using a combination of three nodes (SA, AV and HP), the mathematical expression of the ECG signal is given by

$$
X = ECG = X_1 + X_3 + X_5 \tag{3}
$$

With

Citation: Fonkou RF, Lima GS, Savi MA. On the Heart Rhythm Analysis by an Intelligent Control Method Using Artificial Neural Networks: Analytical Study and Electronic Simulation. J Cardiovasc Med Cardiol. 2026;13(3):42-72. Available from: https://dx.doi.org/10.17352/2455-2976.000242

$$\begin{cases} X_1 = \dfrac{a_0}{3} + a_1 x_1 \\ X_3 = \dfrac{a_0}{3} + a_2 x_3 \\ X_5 = \dfrac{a_0}{3} + a_3 x_5 \end{cases} \quad (4)$$

Where a_0, a_1, a_2 and a_3 are constant parameters. In addition, it is possible to write:

$$\dot{x} = \frac{d(ECG)}{dt} = a_1 x_2 + a_2 x_4 + a_3 x_6 \quad (5)$$

Considering the equations of the system (1) adimensioned, the parameters to conform with them are given by: $\bar{t}[s] : \bar{t} = a_\tau t$ where $[a_\tau] = s$. It can also be considered as the ratio between the experimental value and the numerical value : $\dfrac{\text{mean}(RR_{exp})}{\text{mean}(RR_{num})}$. Here the external excitations are considered as harmonics: $F_{SA}(t) = \rho_{SA}\sin(\omega_{SA} t), F_{AV}(t) = \rho_{AV}\sin(\omega_{AV} t)$ and $F_{HP}(t) = \rho_{HP}\sin(\omega_{HP} t)$. All simulations consider $a_\tau = 1.0mV, a_1 = 2.0mV, a_2 = 0.01mV$ and $a_3 = 0.15mV$, for all the simulations, we will take as initial conditions : $x_{1,3,5} = 0.01$ and $\dot{x}_{1,3,5} = 0.04$.

Note that the model parameters are estimated from the same real ECG data and can be either deterministic or non-deterministic. In deterministic situations, each rhythm is considered to be associated with a set of parameters, and a change in that rhythm is attributed to a change in those parameters. In other words, a pathological rhythm can be understood as resulting from a change in these parameters. In contrast, nondeterministic situations involve random variations in the parameters that can lead to pathological rhythms. t should also be noted that the constants of the coupled Duffing model are physiologically grounded: the natural frequencies ω_i reproduce the intrinsic automaticity of the SA node (1 Hz), the AV node (0.7 Hz), and the His-Purkinje system ($0.4H_Z$) [58]. The delays τ_i correspond to the PR interval of 0.1 s and the QRS interval of 0.08 s measured on a 12 -lead ECG [59]. The coupling coefficients k_{i-j} model the conductances of connexin-mediated junctions, the reduction of which explains AV block [60]. The Duffing nonlinearities α_i and a_i (a_0, a_1, a_2 and a_3) are justified by the nonlinear current-voltage relationship of the voltage-dependent Na^+, Ca^+, K^+ channels [28]. The synthetic ECG generated is therefore the weighted sum of the three oscillators, in accordance with the principle of superposition of cardiac dipoles [61].

It should also be noted that changing the value of a constant alters the nature of the ECG signal in accordance with the clinical case. For example, a decrease in one of the k_{i-j} values can lead to a prolongation of the PR interval, which would imply the onset of AV block. An increase or decrease in α_i can alter the T wave and, in some cases, lead to hyperkalemia.

All of these analyses were presented in the manuscript, and the parameter changes were provided in Table 2 of the manuscript, yielding the curves shown in Figures 7-10.

This transforms the mathematical model into a physiological model. Furthermore, considering the equation for a cardiac oscillator given by:

$$\dot{x}_{2i} = F_i(t) - \alpha_i x_{2i}\left(x_{1i} - v_{i_1}\right)\left(x_{2i} - v_{i_2}\right) - \omega\frac{x_{1i}\left(x_{1i} - d_i\right)\left(x_1 - e_i\right)}{d_i e_i}$$

α_i modifies the shape of the pulse, resulting in a change in the refractory period. e_i Controls the diastolic period; the self-oscillatory nature is maintained whenr $v_{i1}v_{i2} < 0$. Varying v_{i1} and v_{i2} allows the resting potential to be lowered or raised, which decreases or increases the frequency of action potential generation. This occurs without affecting the amplitude of the oscillations [62] $F_i(t)$ is the external stimulus that originates from a spatiotemporal stimulus and is therefore considered a reduced-order representation of spatiotemporal aspects

Citation: Fonkou RF, Lima GS, Savi MA. On the Heart Rhythm Analysis by an Intelligent Control Method Using Artificial Neural Networks: Analytical Study and Electronic Simulation. J Cardiovasc Med Cardiol. 2026;13(3):42-72. Available from: https://dx.doi.org/10.17352/2455-2976.000242

Fixed points analysis

The search and analysis of equilibrium points is carried out by considering the model in its unidirectional connection state. In this case, its conceptual model is given in figure 3, the mathematical model characterizing it is given by equation (6) and the parameters for obtaining normal dynamics in Table 1, Figure 3.

$$\begin{cases} \ddot{y}_{x_1} = x_2 \\ \ddot{y}_{x_2} = -\alpha_{SA} x_2 \left(x_1 - v_{SA_1}\right)\left(x_2 - v_{SA_1}\right) - \omega \dfrac{x_1 \left(x_1 - d_{SA}\right)\left(x_1 - e_{SA}\right)}{d_{SA} e_{SA}} \\ \ddot{y}_{x_3} = x_4 \\ \dot{x}_4 = -\alpha_{AV} x_4 \left(x_3 - v_{AV_1}\right)\left(x_3 - v_{AV_1}\right) - \dfrac{x_3 \left(x_3 - d_{AV}\right)\left(x_3 - e_{AV}\right)}{d_{AV} e_{AV}} - k_{SA-AV}\left(x_3 - x_3^3\right) \\ \quad + k^{\tau}_{SA-AV}\left(x_1^{\tau_{SA-AV}} + \left(x_1^{\tau_{SA-AV}}\right)^3\right) \\ \ddot{y}_{x_5} = x_6 \\ \dot{x}_6 = -\alpha_{HP} x_6 \left(x_5 - v_{HP_1}\right)\left(x_5 - v_{HP_1}\right) - \dfrac{x_5 \left(x_5 - d_{HP}\right)\left(x_5 - e_{HP}\right)}{d_{HP} e_{HP}} - k_{AV-HP}\left(x_5 - x_5^3\right) \\ \quad + k^{\tau}_{AV-HP}\left(x_3^{\tau_{AV-HP}} + \left(x_3^{\tau_{AV-HP}}\right)^3\right) \end{cases} \tag{6}$$

Fixed points

The fixed points or equilibrium points of this system are obtained by solving the system (7).

$$\begin{cases} \ddot{y}_{x_1} = 0 \\ \ddot{y}_{x_2} = 0 \\ \dot{x}_3 = 0 \\ \dot{x}_4 = 0 \\ \dot{x}_5 = 0 \\ \dot{x}_6 = 0 \end{cases} \tag{7}$$

(7) To facilitate the search for fixed points, a Taylor expansion [63] is proposed. The delay terms make the system more complex, but this allows for more manageable equations. This expression is given in equation (8) and the new system in equation (9).

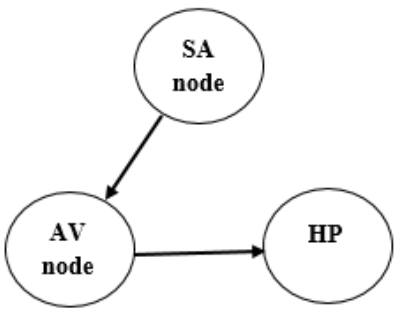

Figure 3: Conceptual model of normal functioning of the heart.

Citation: Fonkou RF, Lima GS, Savi MA. On the Heart Rhythm Analysis by an Intelligent Control Method Using Artificial Neural Networks: Analytical Study and Electronic Simulation. J Cardiovasc Med Cardiol. 2026;13(3):42-72. Available from: https://dx.doi.org/10.17352/2455-2976.000242

$$x(t-T) = x^{T} = x(t) - T\dot{x}(t)$$
$$x_2 = 0 \tag{8}$$

$$\begin{cases} x_1\left(x_1 + d_{SA}\right)\left(x_1 + e_{SA}\right) = 0 \\ x_4 = 0 \\ a_{AV}x_3^3 + b_{AV}x_3^2 + c_{AV}x_3 + k_{AV} = 0 \\ x_6 = 0 \\ a_{HP}x_5^3 + b_{HP}x_5^2 + c_{HP}x_5 + k_{HP} = 0 \end{cases} \tag{9}$$

With

$$\omega_{SA} \tag{10}$$

A detailed, step-by-step derivation of equations (9) and (10) is provided in Appendix A Using Cardran's solution method [64], we obtain 27 equilibrium points, 5 of which are actual equilibrium points, namely:

$$P_1 = (0,0,0,0,0,0,); P_4 = (0,0,-1.48,0,-1.62,0,); P_7 = (0,0,-0.27,0,-0.18,0,)$$
$$P_{10} = (-2,0,-2.76,0,-1.27,0,); P_{19} = (-3,0,-3.6,0,-3.8,0)\,And\,22$$

complex equilibrium points, namely:

$$P_2 = (0,0,0,0,-0.46 + 1.22i,0,); P_3 = (0,0,0,0,-0.46 - 1.22i,0,); P_5 = (0,0,-1.48,0,0.35 + 1.64\mathrm{i},\ 0,)$$

$$P_6 = (0,0,-1.48,0,0.35 - 1.64i,0,); P_8 = (0,0,-0.27,0,-0.37 + 1.2i,0,); P_9 = (0,0,-0.27,0,-0.37 - 1.2\mathrm{i},\ 0,)$$

$$P_{11} = (-2,0,-2.76,0,0.17 + 1.45i,0,); P_{12} = (-2,0,-2.76,0,0.17 - 1.45i,0,); P_{13} = (-2,0,0.5 + 1.7i\ \ 0,0.1 + 1.7i,0$$

$$P_{16} = (-2,0,0.5 - 1.7i,0,0.1 - 1.7i,0,); P_{17} = (-2,0,0.5 - 1.7i,0,-1.5 + 0.33i,0,$$

$$P_{18} = (-2,0,0.5 - 1.7i,0,-0.5 + 1.4i,0,); P_{20} = (-3,0,-3.6,0,1.46 + 3.3i,0,); P_{21} = (-3,0,-3.6,0,1.46 - 3.3i,0,)$$

$$P_{22} = (-3,0,0.94 + 2.5i,0,0.58 + 2.5i,0,); P_{23} = (-3,0,0.94 + 2.5i,0,-2.6 - 0.37i,0,$$

$$P_{24} = (-3,0,0.94 + 2.5i,0,1.14 - 2.15i,0,); P_{25} = (-3,0,0.94 - 2.5i,0,0.58 - 2.5i,0,$$

$$P_{26} = (-3,0,0.94 - 2.5i,0,-2.6 + 0.37i,0,); P_{27} = (-3,0,0.94 - 2.5i,0,1.14 + 2.15i,0,)$$

The stability analysis is made by computing the Jacobean matrix of the system (6). This matrix is given by equation (11).

$$J = \begin{bmatrix} 0 & 1 & 0 & 0 & 0 & 0 \\ B_1 & B_2 & 0 & 0 & 0 & 0 \\ 0 & 0 & 0 & 1 & 0 & 0 \\ B_3 & B_4 & B_5 & B_6 & 0 & 0 \\ 0 & 0 & 0 & 0 & 0 & 1 \\ 0 & 0 & B_7 & B_8 & B_9 & B_{10} \end{bmatrix} \tag{11}$$

With

Citation: Fonkou RF, Lima GS, Savi MA. On the Heart Rhythm Analysis by an Intelligent Control Method Using Artificial Neural Networks: Analytical Study and Electronic Simulation. J Cardiovasc Med Cardiol. 2026;13(3):42-72. Available from: https://dx.doi.org/10.17352/2455-2976.000242

$$\begin{cases} B_1 = -2\alpha_{SA}x_1x_2 + \alpha_{SA}\left(v_{SA_1} + v_{SA_2}\right)x_2 - \dfrac{3}{d_{SA}e_{SA}}x_1^2 - \dfrac{2}{d_{SA}e_{SA}}\left(d_{SA} + e_{SA}\right)x_1 - 1 \\ B_2 = -\alpha_{SA}x_1^2 + \alpha_{SA}\left(v_{SA_1} + v_{SA_2}\right)x_1 - \alpha_{SA}v_{SA_1}v_{SA_2} \\ B_3 = k_{SA-AV}^{\tau}\left(1 + 3x_1^2 - 6\tau_{SA-AV}x_1x_2 + 3\tau_{SA-AV}^2x_2^2\right) \\ B_4 = k_{SA-AV}^{\tau}\left(-\tau_{SA-AV} - 3\tau_{SA-AV}x_1^2 + 6\tau_{SA-AV}^2x_1x_2 - 3\tau_{SA-AV}^3x_2^2\right) \\ B_5 = -2\alpha_{AV}x_3x_4 + \alpha_{AV}\left(v_{AV_1} + v_{AV_2}\right)x_4 - \dfrac{3}{d_{AV}e_{AV}}x_3^2 - \dfrac{2}{d_{AV}e_{AV}}\left(d_{AV} + e_{AV}\right)x_3 - 1 - k_{SA-AV}\left(1 + 3x_3^2\right) \\ B_6 = -\alpha_{AV}x_3^2 + \alpha_{AV}\left(v_{AV_1} + v_{AV_2}\right)x_3 - \alpha_{AV}v_{AV_1}v_{AV_2} \\ B_7 = k_{AV-HP}^{\tau}\left(1 + 3x_3^2 - 6\tau_{AV-HP}x_3x_4 + 3\tau_{AV-HP}^2x_4^2\right) \\ B_8 = k_{AV-HP}^{\tau}\left(-\tau_{AV-HP} - 3\tau_{AV-HP}x_3^2 + 6\tau_{AV-HP}^2x_3x_4 - 3\tau_{AV-HP}^3x_4^2\right) \\ B_9 = -2\alpha_{HP}x_5x_6 + \alpha_{HP}\left(v_{HP_1} + v_{HP_2}\right)x_6 - \dfrac{3}{d_{HP}e_{HP}}x_5^2 - \dfrac{2}{d_{HP}e_{HP}}\left(d_{HP} + e_{HP}\right)x_5 - 1 - k_{AV-HP}\left(1 + 3x_5^2\right) \\ B_{10} = -\alpha_{HP}x_5^2 + \alpha_{HP}\left(v_{HP_1} + v_{HP_2}\right)x_5 - \alpha_{HP}v_{HP_1}v_{HP_2} \end{cases} \quad (12)$$

The verification of the Jacobian matrix reductions is provided in Appendix B. By resolving $\mathrm{Det}\left(J - \lambda I_6\right) = 0$, we obtain the characteristic equation (13).

$$b_6\lambda^6 + b_5\lambda^5 + b_4\lambda^4 + b_3\lambda^3 + b_2\lambda^2 + b_1\lambda + b_0 = 0 \quad (13)$$

$$I_6 = \begin{matrix} 1 & 0 & 0 & 0 & 0 & 0 \\ 0 & 1 & 0 & 0 & 0 & 0 \\ 0 & 0 & 1 & 0 & 0 & 0 \\ 0 & 0 & 0 & 1 & 0 & 0 \\ 0 & 0 & 0 & 0 & 1 & 1 \\ 0 & 0 & 0 & 0 & 0 & 1 \end{matrix}$$

is the identity matrix of order 6, and $b_1 = -B_1B_5B_{10} - B_1B_5 - B_5B_2$

$$b_6 = 1; b_5 = -B_2 - B_6 - B_{10}; b_4 = B_2B_6 - B_5 + B_2B_{10} + B_6B_{10} - B_9; b_0 = -B_1B_5B_9$$

$$b_2 = B_1B_5 + B_5B_9 - B_2B_6B_9 - B_1B_6B_{10} - B_2B_5B_{10}$$

$$b_3 = B_1B_6 + B_2B_5 + B_2B_9 + B_6B_9 - B_2B_6B_{10} + B_5B_{10}$$

Using the Ruth-Hurwitz stability criterion, equation (13) gives us 4 stable fixed points and 23 unstable fixed points. The stable fixed points are: P_{19}, P_{20}, P_{21} et $P_{23}.P_{20}$ and P_{21} are asymptotically stable, P_{19} and P_{23} are marginally stable.

For the fixed point P_{19}, we have the following eigenvalues:

$$\lambda_1 = -1.4090; \lambda_2 = -1.2390; \lambda_3 = -1.1526; \lambda_4 = -0.0077; \lambda_5 = 0.0002i; \lambda_6 = -0.0003i$$

For the fixed point P_{20}, we have the following eigenvalues:

$$\lambda_1 = -0.8306 - 1.6664i; \lambda_2 = -1.4094; \lambda_3 = -1.2376; \lambda_4 = -0.0062 - 0.0002i; \lambda_5 = -0.0002 - 0.0003i; \lambda_6 = -0.0003 + 0.0002i$$

For the case of a fixed point P_{21}, the eigenvalues are:

$$\lambda_1 = -0.8306 + 1.6664i; \lambda_2 = -1.4094; \lambda_3 = -1.2376; \lambda_4 = -0.0062 + 0.0002i; \lambda_5 = -0.0002 + 0.0003i; \lambda_6 = -0.0003 - 0.0002i$$

Citation: Fonkou RF, Lima GS, Savi MA. On the Heart Rhythm Analysis by an Intelligent Control Method Using Artificial Neural Networks: Analytical Study and Electronic Simulation. J Cardiovasc Med Cardiol. 2026;13(3):42-72. Available from: https://dx.doi.org/10.17352/2455-2976.000242

On the other hand, the fixed point P_{23}, we have the following eigenvalues:

$$\lambda_1 = -1.2380; \lambda_2 = -0.6149 - 0.6866i; \lambda_3 = -0.3885 - 0.1782i; \lambda_4 = -0.0083 + 0.0009i; \lambda_5 = -0.0002i; \lambda_6 = 0.0003i$$

Normal synthetic ECG

Considering the synthetic model of heart function (Figure 3) and the parameters for obtaining normal rhythms given in Table 1, the synthetic ECG is observed in Figure 4.

Figure 4 shows the synthetic ECG signal obtained by digital simulation. The presence of the five main ECG waves is observed, namely the P waves, the QRS complex and the T wave. A comparison with a signal recovered from a real recording is made [65]. The different dynamics of the SA, AV and HP nodes are given in Figure 5.

Pathological synthetic ECGs

In this section, the presentation of cardiac pathologies obtained when only the sinus node is disturbed in the absence of any control signal ($u = 0$) is described following the mathematical model. None of the parameters of the main system in its normal state

Table 1: Heart system parameters for ECG simulation.

Coupling parameters	SA Oscillator	AV Oscillator	HP Oscillator	Φ parameter
$k_{SA-AV} = 1.2$	$\alpha_{SA} = 14.0$	$\alpha_{AV} = 12.0$	$\alpha_{HP} = 12.0$	$\omega_a = 1$
$k_{AV-HP} = 1.1$	$v_{SA_1} = 0.52$	$v_{AV_1} = 0.01$	$v_{HP_1} = 0.1$	$\omega_b = 1$
$k^{\tau}_{SA-AV} = 1.1$	$v_{SA_2} = -0.5$	$v_{AV_2} = -0.4$	$v_{HP_1} = -1.4$	$\gamma = 0.05$
$k^{\tau}_{AV-HP} = 1.2$	$d_{SA} = 2.0$	$d_{AV} = 3.0$	$d_{HP} = 7.0$	$t_0 = 0.0$
$\tau_{SA-AV} = 0.8$	$e_{SA} = 3.0$	$e_{AV} = 5.91$	$e_{HP} = 1.0$	
$\tau_{AV-HP} = 0.1$				

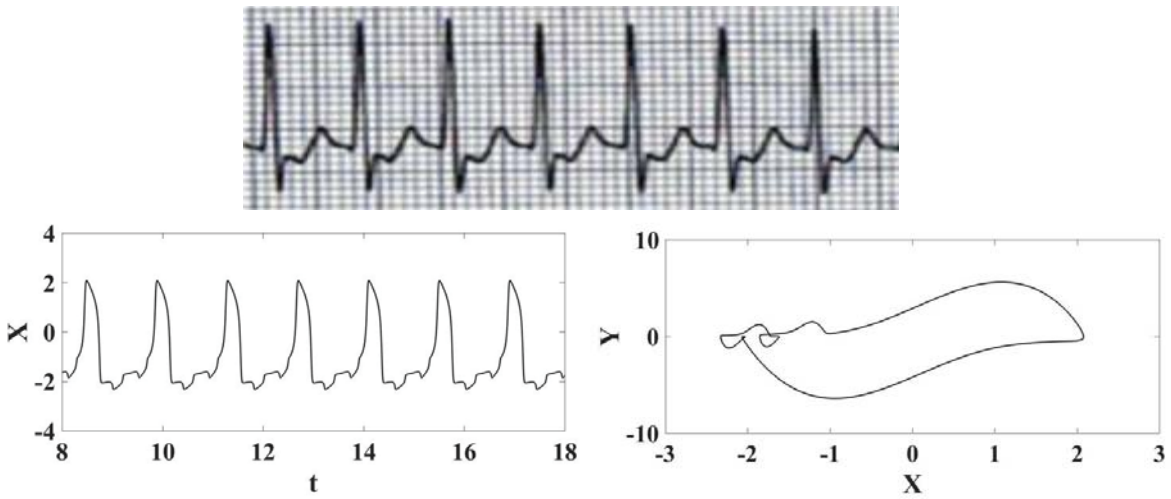

Figure 4: Normal ECG. (a) Experimental recorded ECG signal [60] (b) Synthetic ECG time series; (c) Synthetic ECG state space.

Citation: Fonkou RF, Lima GS, Savi MA. On the Heart Rhythm Analysis by an Intelligent Control Method Using Artificial Neural Networks: Analytical Study and Electronic Simulation. J Cardiovasc Med Cardiol. 2026;13(3):42-72. Available from: https://dx.doi.org/10.17352/2455-2976.000242

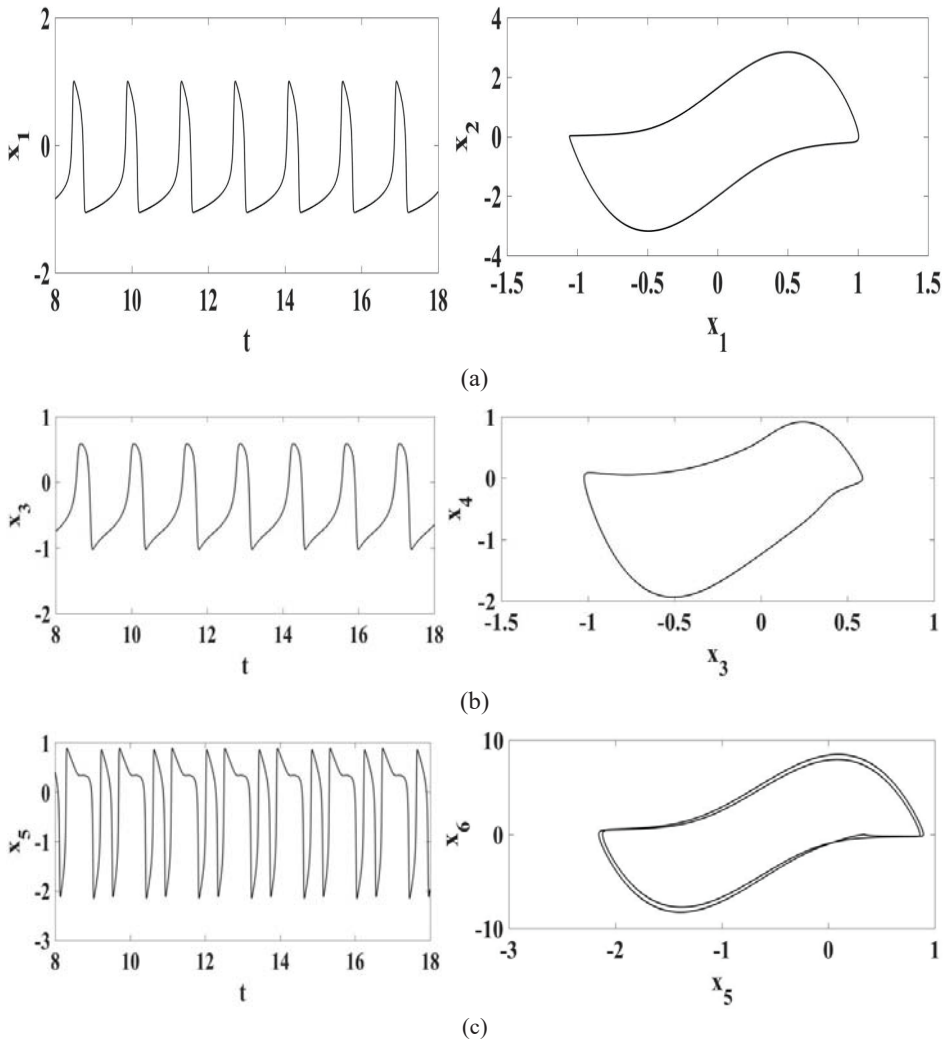

Figure 5: Normal synthetic ECG represented by each one of the oscillator responses in the form of time series and state space. (a) SA node; (b) AV node; (c) HP complex.

are modified. Only external stimulus parameters related to the sinus node are modified. In this case, the system is disturbed only at the level of its sinus node and the other disturbances are not considered since we only wanted to control the heart by following the trajectory of the SA node. According to the values taken by the parameters ρ_{SA} and ω_{SA}, four types of pathologies dangerous for the normal functioning of the heart are highlighted in order to observe the power of our controller. These are ventricular flutter, ventricular fibrillation, atrial fibrillation and atrial flutter. Their conceptual model is given in Figure (6) and the parameters of obtaining these different pathologies are in table 2,

Case of ventricular flutter

Ventricular flutter is a highly intolerable arrhythmia. In this arrhythmia, the ECG shows an equalsized undulation of the QRS complexes, with no isoelectric line between them and no T wave. There is no evidence of any separation between the QRS and the ST-T. During the onset of ventricular flutter, a high heart rate of between 250 and 300/min is noted. As in the case of ventricular fibrillation, an emergency response is required to avoid recurrence, and a therapeutic approach is necessary. Although it can occur spontaneously, supraventricular tachycardia (SVT) is usually the cause of a heart attack.

It is also manifested by a regular appearance of the cardiac rhythm, absence of the P wave, no true QRS complexes, they are widened (> 0.10 seconds) and of sinusoidal shape, a ratio P wave complex QRS not measurable, a PR interval also not measurable [66]. The presence of influx formation due to an ectopic focus on the left and right branches of the His bundle or the Purkinje network (tertiary automatism center) is also observed. In addition, we also note incessant re-entry of the influx at the level of the branches and network of Purkinje or sometimes in the myocardial fibers.

The dynamics of the ECG are given in Figure 7. Figure 7b shows the time series and Figure 7c the state space. The signal of an

Citation: Fonkou RF, Lima GS, Savi MA. On the Heart Rhythm Analysis by an Intelligent Control Method Using Artificial Neural Networks: Analytical Study and Electronic Simulation. J Cardiovasc Med Cardiol. 2026;13(3):42-72. Available from: https://dx.doi.org/10.17352/2455-2976.000242

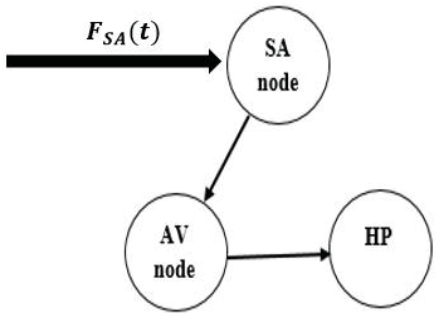

Figure 6: Conceptual model of heart functioning in its pathological state.

Table 2: Heart system parameters for simulation of cardiac pathologies.

SA Oscillator	AV Oscillator	HP Oscillator	Forcing Terms	Coupling Terms	ECG Parameters
Ventricular Flutter					
$\alpha_{SA} = 14.0$	$\alpha_{AV} = 12.0$	$\alpha_{HP} = 12.0$	$\rho_{SA} = 35.6$	$k_{SA-AV} = 1.2$	$a_1 = 2.0$
$v_{SA}^1 = 0.52$	$v_{AV}^1 = 0.01$	$v_{HP}^1 = 0.1$	$\omega_{SA} = 6.94$	$k_{AV-HP} = 1.1$	$a_2 = 0.01$
$v_{SA}^2 = -0.5$	$v_{AV}^2 = -0.4$	$v_{HP}^2 = -1.4$	$\rho_{AV} = 0.0$	$k^{\tau}_{SA-AV} = 1.1$	$a_3 = 0.15$
$d_{SA} = 2.0$	$d_{AV} = 3.0$	$d_{HP} = 7.0$	$\omega_{AV} = 0.0$	$k^{\tau}_{AV-HP} = 1.1$	$a\tau = 1.0$
$e_{SA} = 3.0$	$e_{AV} = 5.91$	$e_{HP} = 1.0$	$\rho_{HP} = 0.0$	$\tau_{SA-AV} = 0.8$	
			$\omega_{HP} = 0.0$	$\tau_{AV-HP} = 0.1$	
Atrial Fibrillation					
$\alpha_{SA} = 14.0$	$\alpha_{AV} = 12.0$	$\alpha_{HP} = 12.0$	$\rho_{SA} = 1.6$	$k_{SA-AV} = 1.2$	$a_1 = 2.0$
$v_{SA}^1 = 0.52$	$v_{AV}^1 = 0.01$	$v_{HP}^1 = 0.1$	$\omega_{SA} = 1.94$	$k_{AV-HP} = 1.1$	$a_2 = 0.01$
$v_{SA}^2 = -0.5$	$v_{AV}^2 = -0.4$	$v_{HP}^2 = -1.4$	$\rho_{AV} = 0.0$	$k^{\tau}_{SA-AV} = 1.1$	$a_3 = 0.15$
$d_{SA} = 2.0$	$d_{AV} = 3.0$	$d_{HP} = 7.0$	$\omega_{AV} = 0.0$	$k^{\tau}_{AV-HP} = 1.2$	$a\tau = 1.0$
$e_{SA} = 3.0$	$e_{AV} = 5.91$	$e_{HP} = 1.0$	$\rho_{HP} = 0.0$	$\tau_{SA-AV} = 0.8$	
			$\omega_{HP} = 0.0$	$\tau_{AV-HP} = 0.1$	
Atrial Flutter					
$\alpha_{SA} = 14.0$	$\alpha_{AV} = 12.0$	$\alpha_{HP} = 12.0$	$\rho_{SA} = 0.66$	$k_{SA-AV} = 1.2$	$a_1 = 2.0$
$v_{SA}^1 = 0.52$	$v_{AV}^1 = 0.01$	$v_{HP}^1 = 0.1$	$\omega_{SA} = 0.35$	$k_{AV-HP} = 1.1$	$a_2 = 0.01$
$v_{SA}^2 = -0.5$	$v_{AV}^2 = -0.4$	$v_{HP}^2 = -1.4$	$\rho_{AV} = 0.0$	$k^{\tau}_{SA-AV} = 1.1$	$a_3 = 0.15$
$d_{SA} = 2.0$	$d_{AV} = 3.0$	$d_{HP} = 7.0$	$\omega_{AV} = 0.0$	$k^{\tau}_{AV-HP} = 1.2$	$a\tau = 1.0$
$e_{SA} = 3.0$	$e_{AV} = 5.91$	$e_{HP} = 1.0$	$\rho_{HP} = 0.0$	$\tau_{SA-AV} = 0.8$	
			$\omega_{HP} = 0.0$	$\tau_{AV-HP} = 0.1$	
Ventricular Fibrillation					
$\alpha_{SA} = 14.0$	$\alpha_{AV} = 12.0$	$\alpha_{HP} = 12.0$	$\rho_{SA} = 30.6$	$k_{SA-AV} = 1.2$	$a_1 = 2.0$
$v_{SA}^1 = 0.52$	$v_{AV}^1 = 0.01$	$v_{HP}^1 = 0.1$	$\omega_{SA} = 6.99$	$k_{AV-HP} = 1.1$	$a_2 = 0.01$
$v_{SA}^2 = -0.5$	$v_{AV}^2 = -0.4$	$v_{HP}^2 = -1.4$	$\rho_{AV} = 0.0$	$k^{\tau}_{SA-AV} = 1.1$	$a_3 = 0.15$
$d_{SA} = 2.0$	$d_{AV} = 3.0$	$d_{HP} = 7.0$	$\omega_{AV} = 0.0$	$k^{\tau}_{AV-HP} = 1.2$	$a\tau = 1.0$
$e_{SA} = 3.0$	$e_{AV} = 5.91$	$e_{HP} = 1.0$	$\rho_{HP} = 0.0$	$\tau_{SA-AV} = 0.8$	
			$\omega_{HP} = 0.0$	$\tau_{AV-HP} = 0.1$	

ECG obtained from a real recording is shown in Figure 7a [67]. It allows a qualitative comparison with the digitally obtained ECG (Figure 7b).

Case of atrial fibrillation

- This is a cardiac arrhythmia characterized by irregular heartbeats due to abnormal acceleration of the heart caused by rhythm disorders [68]. Old age is also a factor favoring the onset of this arrhythmia. The presence of cardiac pathology (hypertension, heart valve disease, etc.), obesity, or obstructive sleep apnea syndrome is also noted. When atrial fibrillation occurs, the atria are the focus of frequent, ineffective electrical impulses, which can levery rapid, jerky contractions (400 to 600 beats / minute) of the atria, resulting in immobility of this part of the heart.

Citation: Fonkou RF, Lima GS, Savi MA. On the Heart Rhythm Analysis by an Intelligent Control Method Using Artificial Neural Networks: Analytical Study and Electronic Simulation. J Cardiovasc Med Cardiol. 2026;13(3):42-72. Available from: https://dx.doi.org/10.17352/2455-2976.000242

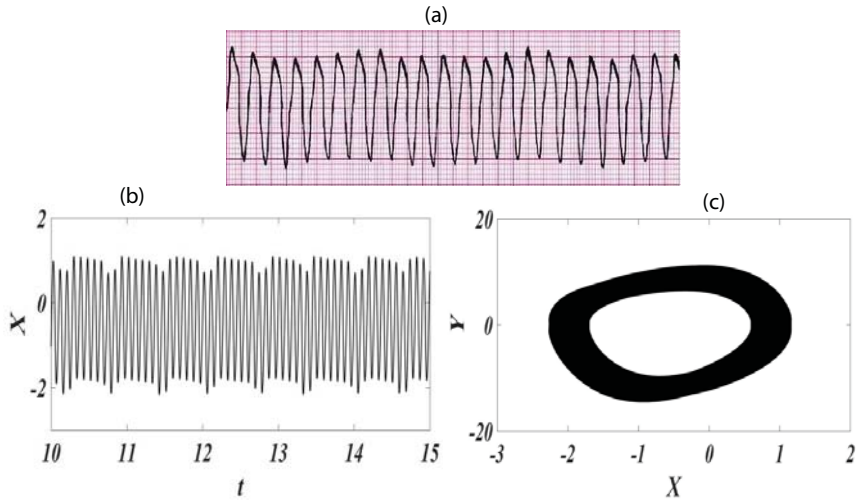

Figure 7: Ventricular flutter ECG signal. (a) Recorded experimental ECG signal [67]; (b) Synthetic ECG time series; (c) Synthetic ECG state space.

- Poor contraction of the atria due to blood stagnation. This is the risk of a cerebral vascular accident due to the propulsion of clots or thrombus in the artery.
- Rapid, irregular beating of the ventricles at around 150 beats per minute (known as tachyarrhythmia) caused by accelerated contraction of the ventricles, located below the atria. Heart failure can occur.

Arrhythmia can also occur in episodes lasting several days, between which a regular heartbeat is observed. It can also be permanent (in which case the irregularity of cardiac contractions is constant).

The ECG dynamics are given in Figure 8. The real ECG recording is observed in figure 8a [67], the time series and the state space of the ECG obtained digitally in figures 8b and 8c. A qualitative comparison is made between Figures 8a and 8b.

Case of atrial flutter

This is a cardiac arrhythmia marked by the presence of a regular rapid rhythm secondary to a macrocircuit of intra-atrial reentry [69]. When palpitations and sometimes asthenia, exertional intolerance, dyspnea, and presyncope are present, these are referred to as symptoms of atrial fibrillation. An ECG helps to better diagnose the condition. This arrhythmia affects people above the age of 60. It accounts for some 60-65% of adult atrial tachycardias (excluding atrial fibrillation). Approximately 1% of people over 80 account for the number of cases of atrial fibrillation.

In the right atrium, there is a macroreentry circuit. Depolarization of the atria is also observed, with a rate of 250 to 300/min (usually 300/min). This frequency does not affect the AV node, and the ventricles are affected by every other atrial activation (2:1 block), inducing a regular ventricular frequency of 150 beats/minute. Occasionally, in AV block, an irregular ventricular rhythm is observed due to beat-to-beat variation. A fixed 3:1, 4:1 or 5:1 block may also be present, although this is generally less frequent.

By medication, prevention of thrombo-embolic events by anticoagulants, etc., the heart rate can be controlled.

For this case, Figure 9 shows the ECG dynamics: Figure 9a we have the ECG signal obtained from a real recording [67], Figure 9b the time series and Figure 9c the state space obtained digitally. A qualitative comparison is made between the digital ECG and the recorded ECG.

Case of ventricular fibrillation

Considered the most severe arrhythmia, ventricular fibrillation is an uncoordinated, potentially lethal series of very rapid, ineffective contractions of the ventricles (lower chambers of the heart), caused by numerous chaotic electrical impulses [70]. In such arrhythmias, one observes very weak or absence of contraction on the part of the ventricles, resulting in very rapid, asynchronous pulsations. One of the consequences is cardiac arrest due to the complete cessation of blood flow. The heart frequency is constantly above 300, with discrete QRS complexes on the electrocardiogram.

Age is an important factor in the development of ventricular fibrillation. Other factors can also be a cause of ventricular fibrillation, including diabetes, hypertension, and underlying heart disease. Major consequences include heart failure and CVA.

Citation: Fonkou RF, Lima GS, Savi MA. On the Heart Rhythm Analysis by an Intelligent Control Method Using Artificial Neural Networks: Analytical Study and Electronic Simulation. J Cardiovasc Med Cardiol. 2026;13(3):42-72. Available from: https://dx.doi.org/10.17352/2455-2976.000242

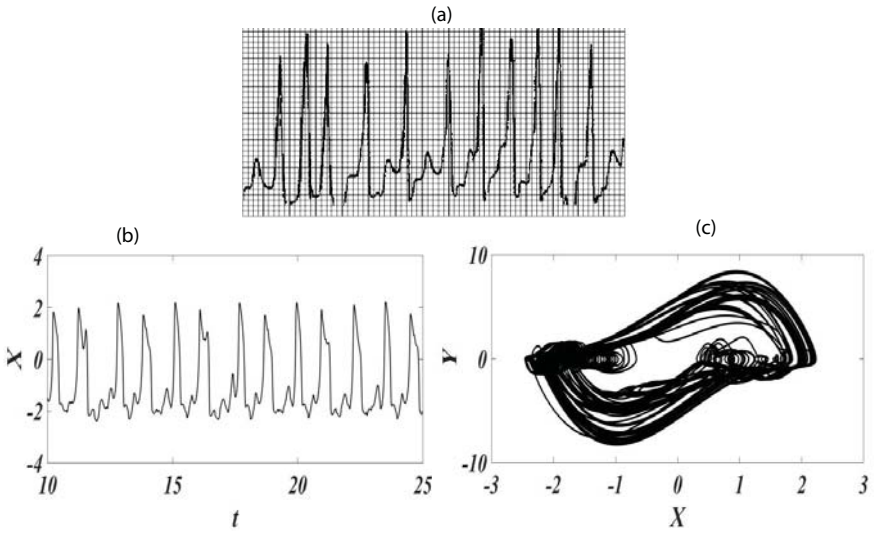

Figure 8: Atrial fibrillation ECG signal. (a) Recorded experimental ECG signal [67]; (b) Synthetic ECG time series. (c) Synthetic ECG state space.

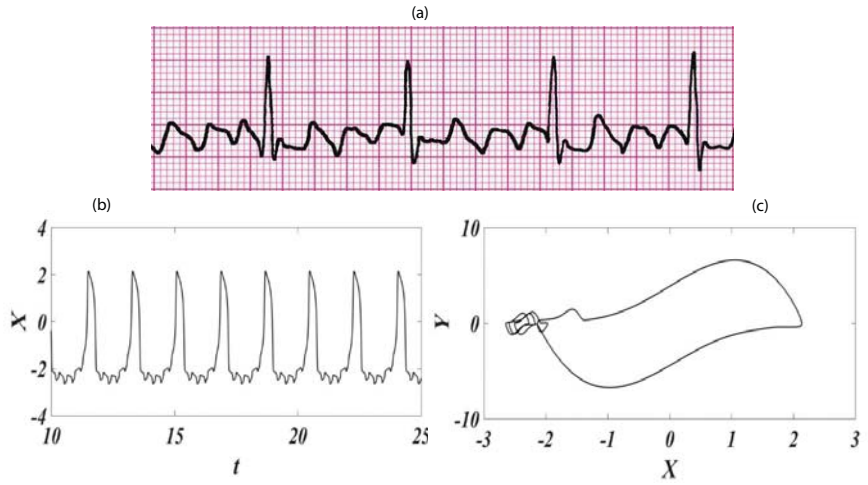

Figure 9: Atrial flutter ECG signal. (a) Recorded experimental ECG signal [67]; (b) Synthetic ECG time series. (c) Synthetic ECG state space.

For this case, Figure 10 shows the ECG dynamics: Figure 10a present the ECG signal obtained from a real recording [67], Figure 10b the time series and Figure 10c the state space obtained digitally. A qualitative comparison is made between the digital ECG and the recorded ECG.

Controller

Recent work on control strategies shows a wide variety of intelligent control systems, used in the control of chaotic systems [71,72], robotic systems [73], under-actuated systems [69], also for the control of unexpected dynamics in non-linear systems [74]. In cardiac systems, their particularity lies in their ability to pick up cardiac signals, analyze them and then ask the controller to act [41]. In order to prevent the heart from being blocked, the systems used as controllers do not apply permanent control. They act only when they observe an abnormal rhythm, and then cease to act once the heart has returned to its normal operating state.

In order to return the heart to its normal functioning state when confronted with external disturbances that could lead it to a pathological operating state, an intelligent controller is implemented. It consists in tracking the trajectory of the SA node signals (in order to stabilize the ECG), the general operation depending only on the state to be controlled and its derivatives (generally the first derivative), and the calculation of the tracking error. The mathematical expression of this controller is given below by equation (14):

$$\ddot{x}SA = g + b\_estu + \rho \quad (14)$$

With u the control signal likely to act on the sinus node in the event of an abnormal heart functioning. The vector field part of the system (1) is represented by g. The hidden dynamics and other specifics of the heart rhythm are represented by p. The controlled

Citation: Fonkou RF, Lima GS, Savi MA. On the Heart Rhythm Analysis by an Intelligent Control Method Using Artificial Neural Networks: Analytical Study and Electronic Simulation. J Cardiovasc Med Cardiol. 2026;13(3):42-72. Available from: https://dx.doi.org/10.17352/2455-2976.000242

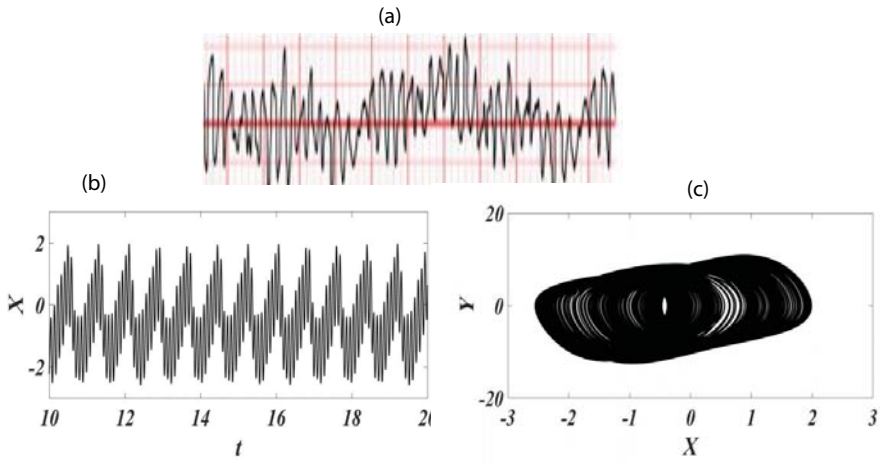

Figure 10: Ventricular fibrillation ECG signal. (a) Recorded experimental ECG signal [67]; (b) Synthetic ECG time series; (c) Synthetic ECG state space.

states are ($x_{SA}, \dot{x}_{SA}$). Using the feedback linearization method [41], the control signal obtained by a combination of feedback errors, desired states, and estimation of the unknown dynamics is given by:

$$u = \left(-g\_est + \ddot{x}SAd - 2\lambda esA - \lambda 2esA - \rho\_est\right) / b\_est \tag{15}$$

Where g_est, b_est and $p\_$ est are the estimates of g,b and p respectively, the feedback error is $e_{SA} = x_{SA} - x_{SAd}$, its first derivative is $e_{S\dot{A}}, x_{SAd}$ is the desired state of the sinus node, and being the control parameter. Replacing u by its expression in equation (14) gives

$$e_{S\ddot{A}} + 2\lambda e_{S\dot{A}} + \lambda^2 e_{SA} = \tilde{p} \tag{16}$$

Equation (16) is obtained by considering all modeling uncertainties are correctly represented by p, and also assuming that $g = g\_est . \tilde{\rho} = \rho - \rho\_est$ is the approximation error.

Using the principle of the sliding mode method, the linear combination of feedback errors is given by

$$s\left(x_{SA}, \dot{x}_{SA}\right) = e_{S\dot{A}} + \lambda e_{SA} \tag{17}$$

It is found that if $s = 0$, a first-order differential equation whose states e_{SA} and $e_{S\dot{A}}$ will converge to zero with a speed co-controlled by λ is obtained, i.e. the more lambda increases, the more the feedback errors converge to zero. From equation (17), the closed-loop dynamics (Equation (16)) becomes:

$$\dot{s} + \lambda s = \tilde{p} \tag{18}$$

It is known that any approximation can be performed using radial basis function (RBF) networks. Using the desired degree of accuracy, an approximation of p is given by $\rho\left(x_{SA}, \dot{x}_{SA}, t\right) = \rho^{*}\_est\left(s\left(x_{SA}, \dot{x}_{SA}\right)\right) + \epsilon(t)$, with ρ^{*}_est optimal estimation and $|\epsilon(t)| \leq$

Thus, the calculation of uncertainty and estimated unmodeled dynamics is done using the RBF in Figure 11. Its expression is:

$$\rho\_est = \text{dot}(W, \varpi)$$

Where $W = \left[W_1 \cdots W_n\right]$ is the weight vector and $\varpi = \left[\varpi_1 \cdots \varpi_n\right]$ represents the vector of activation functions ϖ_i, n being the number of neurons in the hidden layer. The dot function calculates uncertainty and estimated unmodeled dynamics: an internal

Citation: Fonkou RF, Lima GS, Savi MA. On the Heart Rhythm Analysis by an Intelligent Control Method Using Artificial Neural Networks: Analytical Study and Electronic Simulation. J Cardiovasc Med Cardiol. 2026;13(3):42-72. Available from: https://dx.doi.org/10.17352/2455-2976.000242

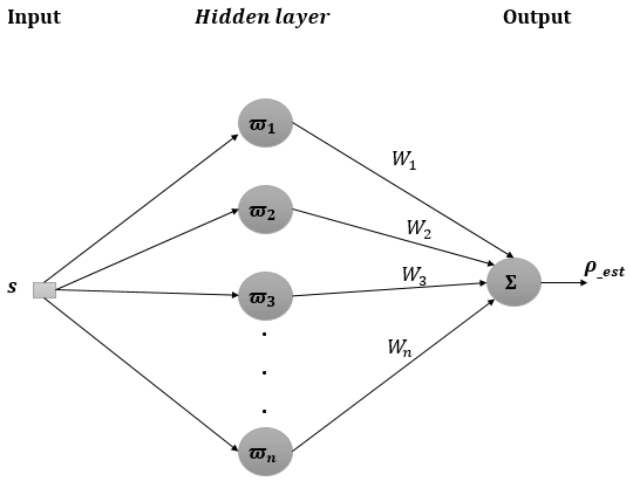

Figure 11: Radial basis function network with one input, n neurons in the hidden layer and one output.

product of the weight neural network and the activation function

The activation function at each neuron in the neural network is similar to a Gaussian distribution and given by the equation (19)

$$\varpi(i) = e^{-0.5\left(\frac{s-C(i)}{\phi(i)}\right)^2} \tag{19}$$

Where $C(i)$ and $\phi(i)$ respectively represent the centers and widths of the activation function By applying s to the input, the order of complexity of the neural network is reduced and made sufficiently flexible, which allows it to be easily inserted into intelligent systems for cardiac rhythm control. A study of the bounding and convergence of the *s* and *W* signals is carried out using Lyapunov-type stability. For this purpose, a difference between the actual weight vector and the optimal weight vector, respectively, *W* and W^+ is define by $\delta = W - W^*$

Knowing that $\tilde{\rho} = \rho - \rho\_est$, with $\rho = \rho^*\_est + \epsilon$, and $\rho\_est = \text{dot}(W, \varpi) = W^T \varpi$. Thus equation (18) takes the form :

$$\begin{aligned} &\dot{s} + \lambda s = \rho - \rho\_est \\ &\rho\_^*est + \epsilon - \rho\_est \\ &= -\left[W - W^*\right]^T \varpi + \epsilon \\ &= -\delta^T \varpi + \epsilon \end{aligned} \tag{20}$$

From equation (20), we obtain the differential equation (21) given by:

$$\dot{s} = -\lambda s - \delta^T \varpi + \epsilon \tag{21}$$

Equation (21) confirms the influence of approximation errors on the dynamic behavior of the system when operating in a closed loop. Hence the interest in integrating a neural network capable of making a universal estimate [71] for which the weights can be known on-line.

Suppose a positive function U defined by the equation (22)

$$U(t) = \frac{1}{2}s^2 + \frac{1}{\mu}\delta^T \delta \tag{22}$$

Where μ is the learning rate. For $\mu = 0$, neural network learning is disabled and only the FBL scheme is applied. For $U > 0, s \neq 0$ and $W > W^*$. For $U = 0, s = 0$ and $W = W^*$ Assuming $W^* = C$ ste, $\delta = \dot{W}$ and *U* is given by:

Citation: Fonkou RF, Lima GS, Savi MA. On the Heart Rhythm Analysis by an Intelligent Control Method Using Artificial Neural Networks: Analytical Study and Electronic Simulation. J Cardiovasc Med Cardiol. 2026;13(3):42-72. Available from: https://dx.doi.org/10.17352/2455-2976.000242

$$U(t) = s\dot{s} + \mu^{-1}\delta^T W$$
$$= -s\left[\lambda s + d_t\delta^T \varpi - \epsilon\right] + \mu^{-1}\delta^T W$$
$$= -s[\lambda s - \epsilon] + \mu^{-1}\delta^T [W - \mu s\varpi] \quad \textit{Initializing}$$

W for $W = \mu s\varpi$, we have:

$$V(t) = -[\lambda s - \epsilon]s \le -[\lambda \mid s \mid -\epsilon] \mid s \mid \tag{23}$$

From equation (23) it can be seen that W is only limited for $\mid s \mid \le / \lambda$. Using the projection algorithm studied in [72], the limit problem of is guaranteed and its domain of definition is taken equal to $Df = W$

$$\left\{W \in IR^n : \text{dot}(W,W) \le \eta\right\} :$$
$$\dot{W} = \begin{cases} \mu s\varpi & \textit{if } \| W \| < \eta \textit{ or } \| W \| = \eta \textit{ and } \mu s\,\text{dot}(W,\varpi) \\ \left(I - \dfrac{WW^T}{\text{dot}(W,\varpi)}\right)\mu s\varpi & \textit{otherwise} \end{cases} \tag{24}$$

Where η is the desired upper limit. It is used to control the limit of increase of the weight neural network. So any value of. So any value of $\| W \|$, it will always be less than η, hence $\mid s \mid \le / \lambda$, which implies $- / \lambda \le s \le / \lambda$. By replacing s by its expression taken from equation (9), we obtain equation

$$- / \lambda \le e_{SA\dot{}} + \lambda e_{SA} \le / \lambda \tag{25}$$

The multiplication of equation (25) by $e^{\lambda t}$ gives the equation

$$-e^{\lambda t}(/\lambda) \le \frac{d}{dt}\left(e_{SA}e^{\lambda t}\right) \le e^{\lambda t}(/\lambda)$$

By integrating (26) between 0 and t and multiplying the result $e^{-\lambda t}$, we obtain

$$\lambda_2 \quad SA \quad \lambda_2 \quad SA \quad \lambda_2 \quad SA \quad \lambda_2 \quad (27) - — + [e$$

For $t \to \infty$ equation (27) results in

$$e \le - + [e \qquad (0) - -]e - \lambda t$$
$$-\lambda^2 \le e_{SA} \le \frac{\lambda^2}{} \tag{28}$$

Inserting (28) into (25) gives :

$$-\frac{2}{\lambda} \le \dot{e}_{SA} \le \frac{2}{\lambda} \tag{29}$$

Equation (29) leads to the conclusion that the exponential convergence of the tracking error to the closed region $\phi = \left\{\left(e_{SA}, \dot{e}_{SA}\right) \in IR^2 : \left|e_{SA}\right| \le \frac{\varepsilon}{\lambda^2} \text{ et } \left|\dot{e}_{SA}\right| \le \frac{2\varepsilon}{\lambda}\right\}$ is guaranteed by the controller

Controlled dynamics

In this section, the results obtained digitally after implementation of the control are presented. The sampling frequency of the signals obtained is taken to be 100 Hz. To obtain the numerical results, the controller is programmed to follow the disturbed trajectories of the SA node, since in its disturbed state, the heart operates in pathological behavior (Figure 5). To normalize the system, a text file with the desired SA node signals extracted from a normal rhythm (from previous simulations) is read in. Since the sinus node is the seat of the electrical impulse, because it takes information from the brain and adapts the heart rate according to the body's needs, the

Citation: Fonkou RF, Lima GS, Savi MA. On the Heart Rhythm Analysis by an Intelligent Control Method Using Artificial Neural Networks: Analytical Study and Electronic Simulation. J Cardiovasc Med Cardiol. 2026;13(3):42-72. Available from: https://dx.doi.org/10.17352/2455-2976.000242

electrical impulse from the sinus node will in turn travel through the two atria, contracting them and encouraging the passage of blood to the ventricles. The electrical impulse then reaches the AV node, where it is filtered and slowed down in the event of disruption of the SA node, before reaching the ventricles. The electrical impulse reaching the ventricles contracts them, enabling the right ventricle to propel blood to the lungs and the left ventricle to the rest of the body. By disrupting the sinus node, the course and nature of the electrical impulse through the heart is also disrupted, resulting in cardiac arrhythmias in the heart. In the present case, the pathological rhythms revealed are: ventricular flutter, ventricular fibrillation, atrial flutter or atrial fibrillation.

The learning rate and control parameter are $\mu = 1500$ and $\lambda = 50$ respectively. Taking $g\_est = 0$, it is assumed that the control system is known without any knowledge about the cardiac model. Thus, to handle all neglected dynamic effects ρ_est is studied. The centers and widths of the activation function defined in equation (11) are given by $C = [-K/2.5, -K/5, -K/10, K/10, K/5, K/2.5]$ et, $\phi = [K/2, K/4, K/8, K/8, K/4, K/2]$.K is the proportionality constant for distributing the neural network activation functions and is taken to be $K = 40.0$. The weight vector is initialized to $W = 0$.

His analyses and the results obtained from numerical simulations show that, when the heart is in a situation of ventricular flutter, ventricular fibrillation, atrial fibrillation, or atrial flutter, once the command has been applied, the ECG dynamics show a considerable approximation to normal rhythms. Abnormal rhythms are thus avoided, enabling the heart to pump enough blood to satisfy the body's needs, while stopping the sudden onset of a heart attack.

Figure 12 shows the conceptual model of the heart in its controlled state.

When the control signal u is applied to the system (1) in its sick state, the controlled ECG dynamics are shown in Figures 13-16 respectively. Figure 13 shows those obtained in the case of ventricular flutter. For ventricular fibrillation, they are shown in figure 14. Figure 15 shows the results for atrial fibrillation, and figure 16 for atrial flutter.

Figure 16. Control signal. (b) Uncontrolled synthetic ECG time series. (c) Uncontrolled synthetic ECG state space. (d) Controller synthetic ECG time series. (e) Controller synthetic ECG state space Figures 13-16 show the action of the controller in cardiac arrhythmia situations. The synthetic ECGs show a qualitative and quantitative approximation between controlled and normal dynamics. Both the phase spaces and the time traces clearly show a very strong improvement in the performance of the highlighted control scheme, as well as its ability to replace a pathological cardiac rhythm with a normal one. The proposed intelligent control scheme shows its ability to make abnormal dynamics disappear.

It can be seen from the curves in figures 13-16 that the action of the controller starts at 15 s. Before 15 s, the controller has no effect on the heart. In the case of ventricular flutter, the control signal, once engaged, evolves at a frequency of 2.4 Hz. In ventricular fibrillation, the control signal has a frequency of 7.2 Hz. In atrial fibrillation, the control signal has a frequency of 8.2 Hz. In atrial flutter, a frequency of 0.6 Hz is observed. Whether in ventricular flutter, ventricular fibrillation, atrial fibrillation or atrial flutter, as observed in normal rhythm, the controlled dynamics clearly show the presence of the QRS complex and P and T waves. We also note the disappearance of the R and S peaks, reflecting the controller's skill in solving this problem

Thus, the feedback linearization control (FBL) method with the integration of an artificial neural network is very effective and robust for the control of pathological heartbeats.

Electronic implementation

In this subsection, we present the results obtained by electronic simulation using OrCAD-PSpice software. This is one of the most widely used simulations in electronic product design, whether for PCB design, IC design or other electrical systems. For the analysis of the most important electronic circuits, OrCAD-PSpice seems to be the most suitable simulation. Wired assemblies in this software allow the use of components with values that reproduce real components as effectively as possible. Once the device has been wired,

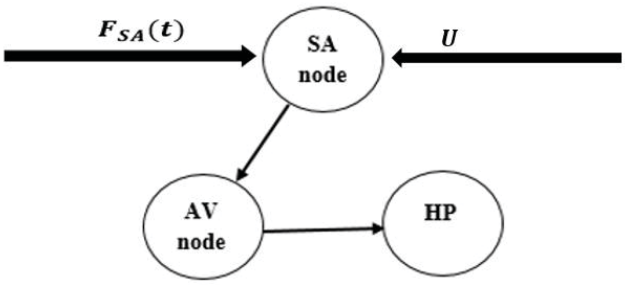

Figure 12: Conceptual model of heart functioning in its pathological state.

Citation: Fonkou RF, Lima GS, Savi MA. On the Heart Rhythm Analysis by an Intelligent Control Method Using Artificial Neural Networks: Analytical Study and Electronic Simulation. J Cardiovasc Med Cardiol. 2026;13(3):42-72. Available from: https://dx.doi.org/10.17352/2455-2976.000242

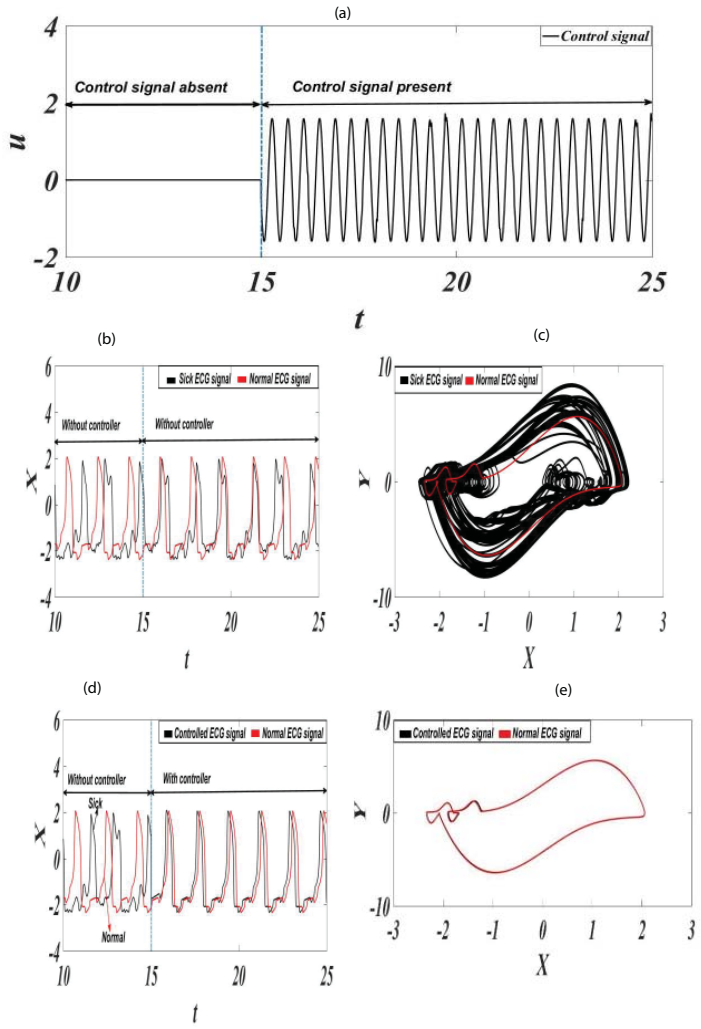

Figure 13: (a) Control signal. (b) Uncontrolled synthetic ECG time series. (c) Uncontrolled synthetic ECG state space. (d) Controller synthetic ECG time series. (e) Controller synthetic ECG state space.

the results can be analyzed in all their facets, using tools as varied as they are sophisticated. A large number of research studies have shown that OrCAD-PSpice is a world reference in the field of circuit design and simulation [4,27], as it possesses some of the most interesting features, including: the possibility of creating virtual components, using manufacturers' data sheets, downloading component libraries.

These include: reducing time wasted in choosing component values before the practical implementation of the system and exploring the advantages of different practical implementation options. Faced with the complexity of creating electronic assemblies whose results can be used to interpret real phenomena, OrCAD-PSpice software helps designers to solve problems at different levels of abstraction, to better understanding the interactions between the various components making up the system.

To implement the mathematical system on the OrCAD-Pspice software, Kirchhoff's and Ohm's laws are used and the system is modeled in the form of differential equations [27]. In this subsection, the dynamics of the system in its state of normal functioning are presented. The system used is the one described by the functional model in Figure 3.

Using electronic equivalence techniques and operational amplifier integration (AOP) principles, the OrCAD-PSpice assembly of the SA oscillator, AV oscillator, and HP oscillator coupled together is shown in Figures 17-19 respectively.

The above circuit implements the analog equivalence of the SA oscillator. It is composed of nine (9) resistors ($R_1SA, R_2SA, R_3SA, R_4SA, R_5SA, R_6SA, \ldots\ldots$, and R_9SA), 2 capacitors (C_1SA and C_2SA), 4 operational amplifiers (TL082), 4 multipliers (AD633/AD), DC voltage sources to power integrated circuits (AOP and multipliers) for some and for others they are used as parameters of the equivalent circuit. We also note an AC power source ($f_{SA}(t)$) used to excite the circuit. Using the

Citation: Fonkou RF, Lima GS, Savi MA. On the Heart Rhythm Analysis by an Intelligent Control Method Using Artificial Neural Networks: Analytical Study and Electronic Simulation. J Cardiovasc Med Cardiol. 2026;13(3):42-72. Available from: https://dx.doi.org/10.17352/2455-2976.000242

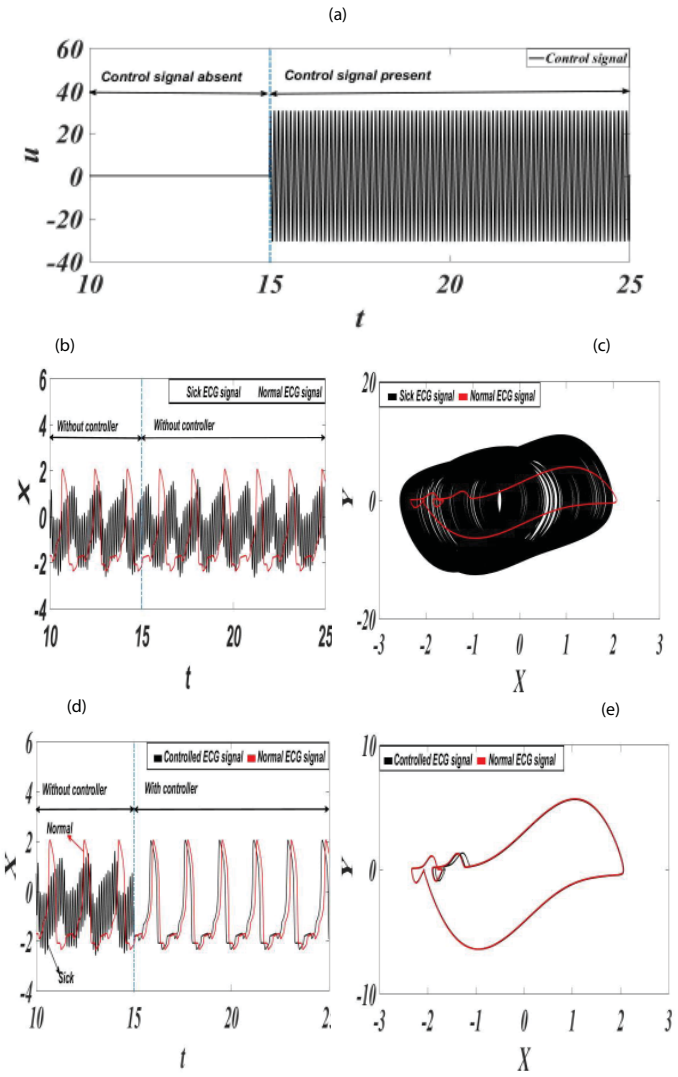

Figure 14: Control signal. (b) Uncontrolled synthetic ECG time series. (c) Uncontrolled synthetic ECG state space. (d) Controller synthetic ECG time series. (e) Controller synthetic ECG state space.

principle of Kirchhoff's laws to Ohm's law, the relationship between the inputs is given below:

$$v_2 = \frac{1}{10}\left(x_1 - V_{1SA}\right)\left(x_1 - V_{2SA}\right) \tag{30}$$

$$B_2 = \frac{1}{100}x_2\left(x_1 - V_{1SA}\right)\left(x_1 - V_{2SA}\right) \tag{31}$$

$$v_3 = \frac{1}{10}\left(x_1 + d_{SA}\right)\left(x_1 + e_{SA}\right) \tag{32}$$

$$B_3 = \frac{1}{100}x_1\left(x_1 + d_{SA}\right)\left(x_1 + e_{SA}\right) \tag{33}$$

$$B_1 = C_{1SA}R_{1SA}\frac{dx_2}{dt} \text{ and } x_2 = C_{2SA}R_{2SA}\frac{dx_1}{dt} \tag{34}$$

$$\frac{\frac{B_1}{R_{7SA}} + \frac{B_2}{R_{5SA}} + \frac{B_3}{R_{6SA}}}{\frac{1}{R_{7SA}} + \frac{1}{R_{5SA}} + \frac{1}{R_{6SA}}} = \frac{R_{9SA}f_{SA}(t)}{R_{9SA} + R_{8SA}} \tag{35}$$

Citation: Fonkou RF, Lima GS, Savi MA. On the Heart Rhythm Analysis by an Intelligent Control Method Using Artificial Neural Networks: Analytical Study and Electronic Simulation. J Cardiovasc Med Cardiol. 2026;13(3):42-72. Available from: https://dx.doi.org/10.17352/2455-2976.000242

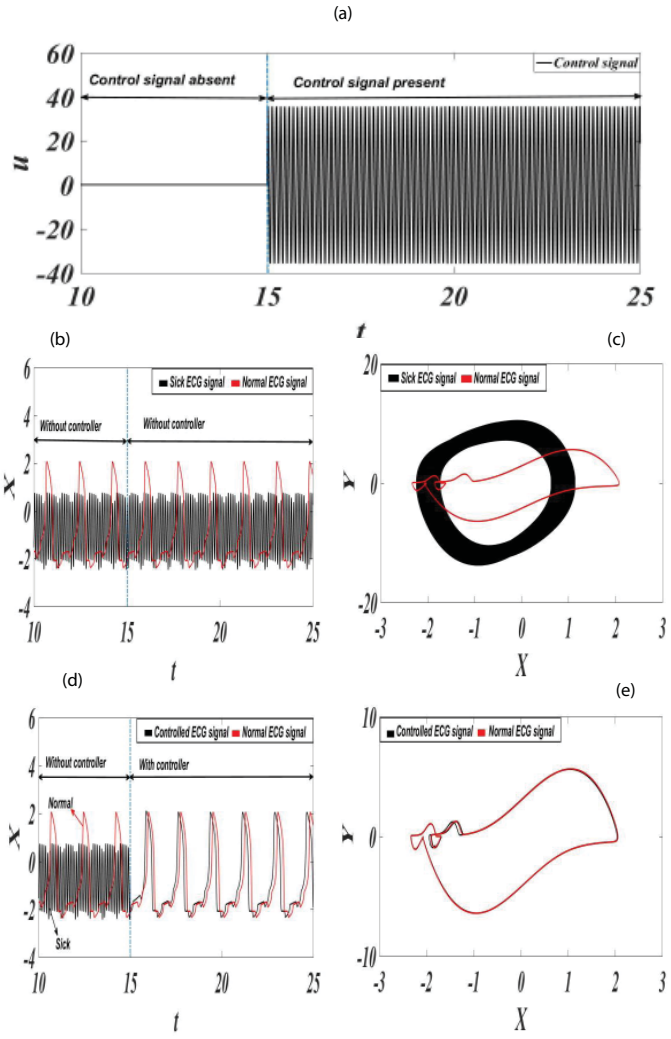

Figure 15: Control signal. (b) Uncontrolled synthetic ECG time series. (c) Uncontrolled synthetic ECG state space. (d) Controller synthetic ECG time series. (e) Controller synthetic ECG state space.

From equation (35), we obtain equation (36) below.

$$B_1 = \frac{R_{7SA}R_{9SA}}{R_{9SA}+R_{8SA}} f_{SA}(t) - \frac{R_{7SA}}{R_{5SA}} B_2 - \frac{R_{7SA}}{R_{6SA}} B_3 \tag{36}$$

The substitution of equations (31) and (33) in (35) gives us equation (37).

$$B_1 = \frac{R_{7SA}R_{9SA}}{R_{9SA}+R_{8SA}} f_{SA}(t) - \frac{R_{7SA}}{100R_{5SA}} x_2 (x_1 - V_{1SA})(x_1 - V_{2SA}) - \frac{R_{7SA}}{100R_{6SA}} x_1 (x_1 + d_{SA})(x_1 + e_{SA}) \tag{37}$$

The relationships between the parameters of the SA node and the data in equation (37) allow us to establish the following correspondences given by equation (38).

$$\frac{R_{7SA}R_{9SA}}{R_{9SA}+R_{8SA}} = 1;\ C_{1SA}R_{1SA} = C_{2SA}R_{2SA} = 1;\ \frac{R_{7SA}}{100R_{5SA}} = \alpha_{SA} \text{ and } \frac{R_{7SA}}{100R_{6SA}} = \frac{1}{e_{SA}d_{SA}} \tag{38}$$

Figure 18. Electronic equivalence of the circuit representing the AV oscillator mounted on OrCAD-PSpice software.

In this case (Figure 18), the analog equivalence is that of the AV oscillator. This figure shows 21 resistors (

Citation: Fonkou RF, Lima GS, Savi MA. On the Heart Rhythm Analysis by an Intelligent Control Method Using Artificial Neural Networks: Analytical Study and Electronic Simulation. J Cardiovasc Med Cardiol. 2026;13(3):42-72. Available from: https://dx.doi.org/10.17352/2455-2976.000242

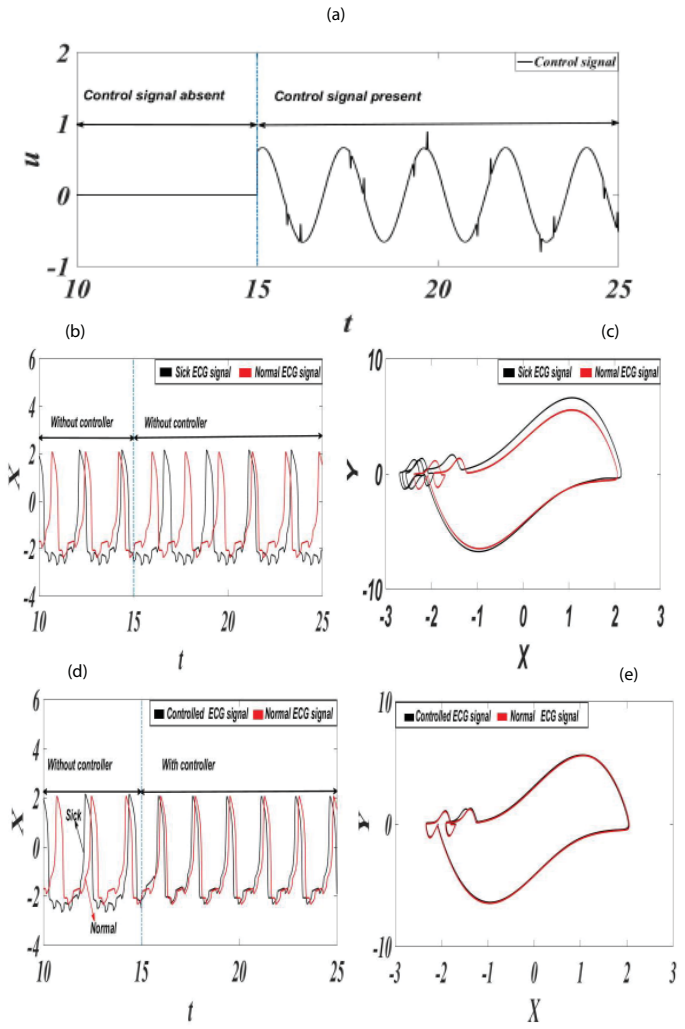

Figure 16: Control signal. (b) Uncontrolled synthetic ECG time series. (c) Uncontrolled synthetic ECG state space. (d) Controller synthetic ECG time series. (e) Controller synthetic ECG state space.

$R_{1AV}, R_{2AV}, R_{3AV}, R_{4AV}, R_{5AV}, R_{6AV}, R_{7AV}, R_{8AV}, \ldots\ldots\ldots\ldots\ldots\ldots, \text{ et } R_{21AV})$, 2 capacitors $(C_{1AV} \text{ et } C_{2AV})$, 8 operational amplifiers (TL082), 8 multipliers (AD633/AD), DC voltage sources to power integrated circuits (AOP and multipliers) for some and others they are used as parameters of the equivalent circuit. The principle of Kirchhoff's laws to Ohm's law is used to establish the relationship between the inputs. The establishment of linear and cubic terms with delay is obtained using Taylor series expansion [68]. For a delayed variable $x(t-T)$, where T is the delay, Taylor's series expansion allows it to be decomposed as follows:

$$x(t-T) = x(t) - T\dot{x}(t) \tag{39}$$

So $x_1(t-T_{SA-AV}) = x_1(t) - T_{SA-AV}x_2(t)$ and $x_3(t-T_{AV-HP}) = x_3(t) - T_{AV-HP}x_4(t)$

Similar reasoning to the previous case (figure 16) gives us the following relationships:

$$vv_2 = \frac{1}{10}(x_3 - V_{1AV})(x_3 - V_{2AV}) \tag{40}$$

$$A_2 = \frac{1}{100}x_4(x_3 - V_{1AV})(x_3 - V_{2AV}) \tag{41}$$

Citation: Fonkou RF, Lima GS, Savi MA. On the Heart Rhythm Analysis by an Intelligent Control Method Using Artificial Neural Networks: Analytical Study and Electronic Simulation. J Cardiovasc Med Cardiol. 2026;13(3):42-72. Available from: https://dx.doi.org/10.17352/2455-2976.000242

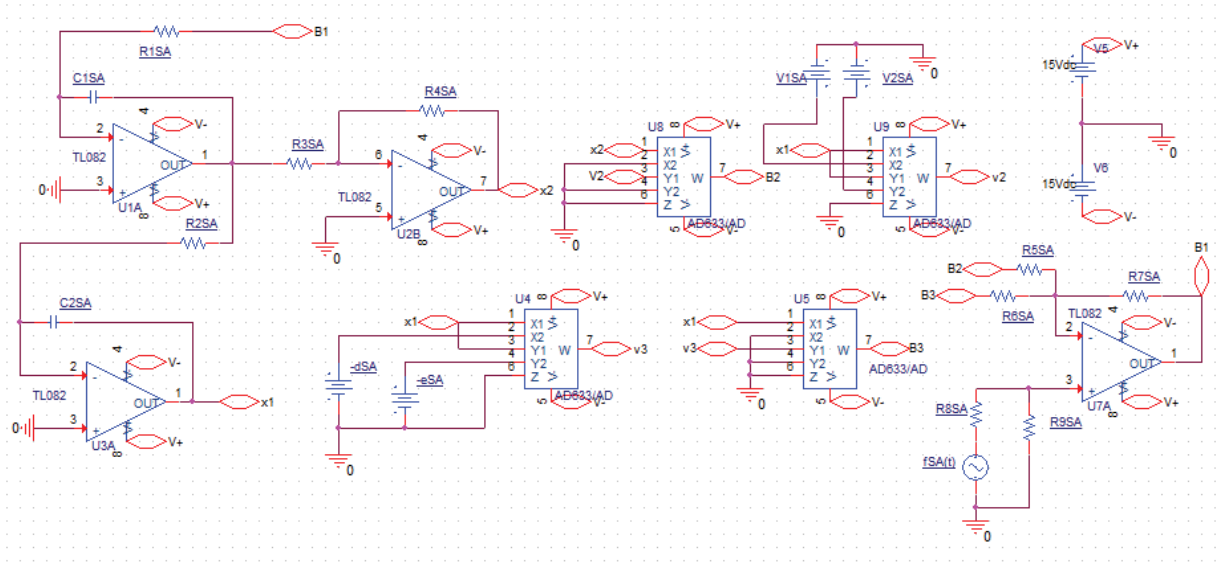

Figure 17: Electronic equivalence of the circuit representing the SA oscillator mounted on OrCAD-PSpice software.

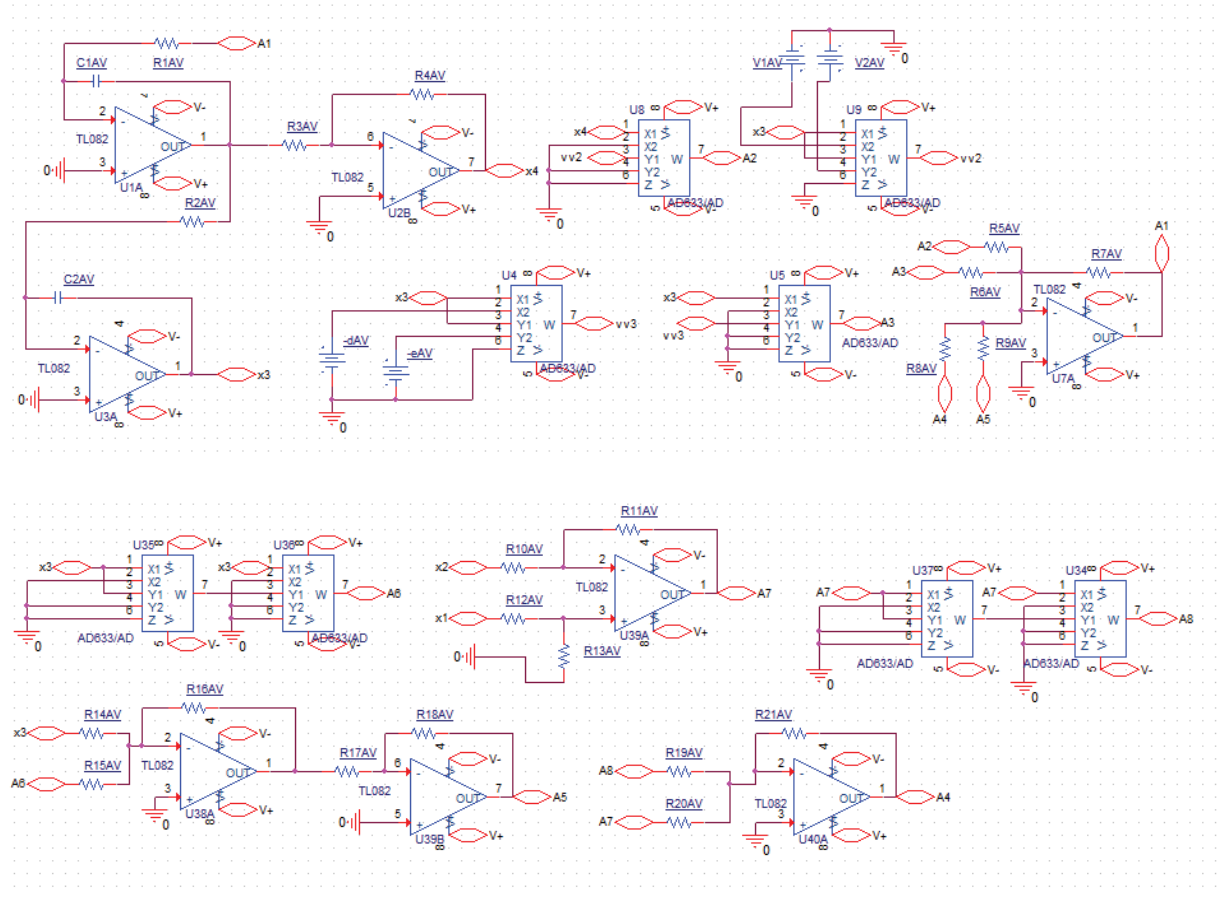

Figure 18: Electronic equivalence of the circuit representing the AV oscillator mounted on OrCAD-PSpice software.

$$vv_3 = \frac{1}{10}\left(x_3 + d_{AV}\right)\left(x_3 + e_{AV}\right) \tag{42}$$

$$A_3 = \frac{1}{100}x_3\left(x_3 + d_{AV}\right)\left(x_3 + e_{AV}\right) \tag{43}$$

Citation: Fonkou RF, Lima GS, Savi MA. On the Heart Rhythm Analysis by an Intelligent Control Method Using Artificial Neural Networks: Analytical Study and Electronic Simulation. J Cardiovasc Med Cardiol. 2026;13(3):42-72. Available from: https://dx.doi.org/10.17352/2455-2976.000242

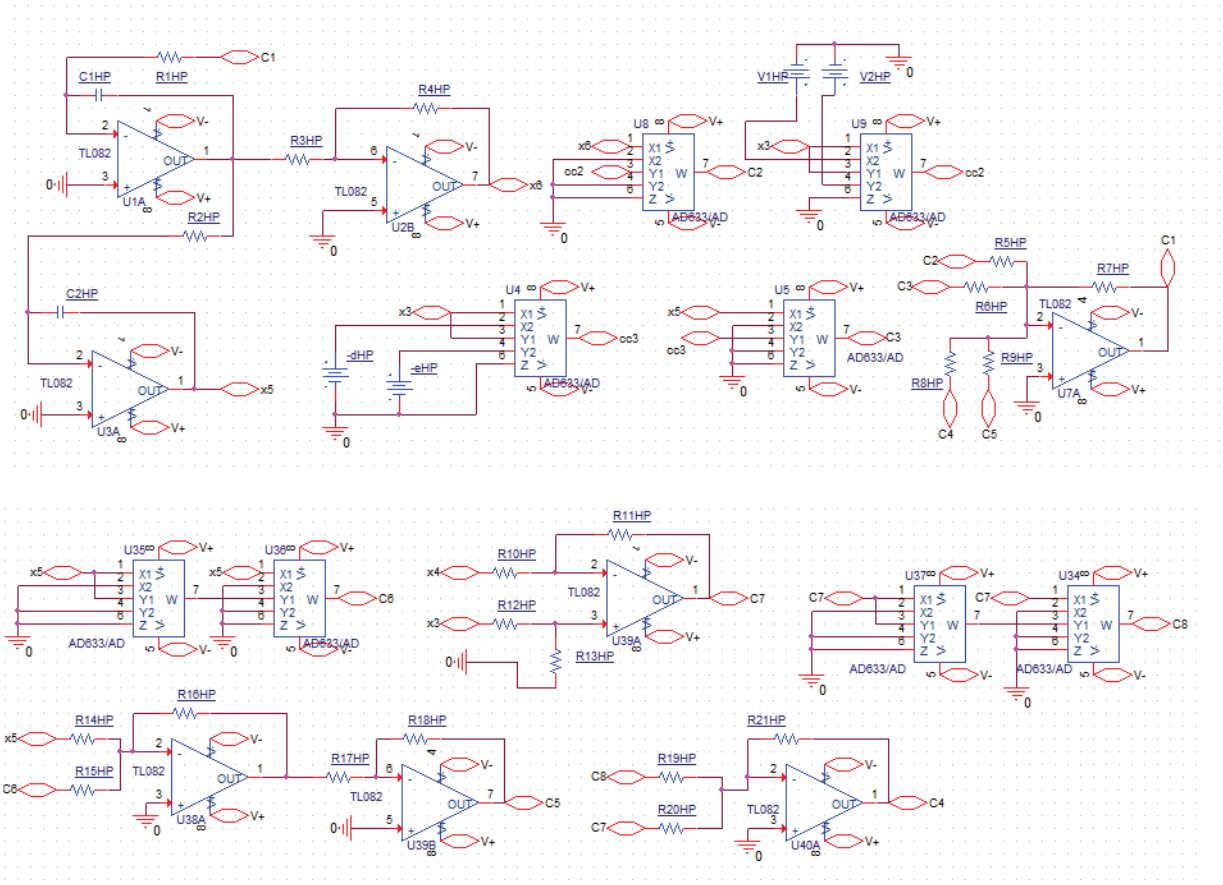

Figure 19: Electronic equivalence of the circuit representing the HP oscillator mounted on OrCAD-PSpice software.

$$A_1 = C_{1AV}R_{1AV}\frac{dx_4}{dt} \text{ and } x_4 = C_{2AV}R_{2AV}\frac{dx_3}{dt} \tag{44}$$

$$A_7 = \frac{R_{11AV}R_{13AV}}{R_{12AV} + R_{13AV}}x_1 - \frac{R_{11AV}}{R_{10AV}}x_2 \tag{45}$$

$$A_8 = \frac{1}{100}\left(\frac{R_{11AV}R_{13AV}}{R_{12AV} + R_{13AV}}x_1 - \frac{R_{11AV}}{R_{10AV}}x_2\right)^3 \tag{46}$$

$$A_6 = \frac{1}{100}x_3^3 \tag{47}$$

$$A_5 = \frac{R_{18AV}R_{16AV}}{R_{17AV}R_{14AV}}x_3 + \frac{R_{18AV}R_{16AV}}{100R_{17AV}R_{15AV}}x_3^3 \tag{48}$$

$$A_4 = -\frac{R_{21AV}}{R_{20AV}}\left(\frac{R_{11AV}R_{13AV}}{R_{12AV} + R_{13AV}}x_1 - \frac{R_{11AV}}{R_{10AV}}x_2\right) - \frac{R_{21AV}}{100R_{19AV}}\left(\frac{R_{11AV}R_{13AV}}{R_{12AV} + R_{13AV}}x_1 - \frac{R_{11AV}}{R_{10AV}}x_2\right)^3 \tag{49}$$

$$A_1 = -\frac{R_{7AV}}{R_{5AV}}A_2 - \frac{R_{7AV}}{R_{6AV}}A_3 - \frac{R_{7AV}}{R_{9AV}}A_5 - \frac{R_{7AV}}{R_{8AV}}A_4 \tag{50}$$

By substituting equations (41), (43), (48) and (49) into (50), we obtain equation (51).

Citation: Fonkou RF, Lima GS, Savi MA. On the Heart Rhythm Analysis by an Intelligent Control Method Using Artificial Neural Networks: Analytical Study and Electronic Simulation. J Cardiovasc Med Cardiol. 2026;13(3):42-72. Available from: https://dx.doi.org/10.17352/2455-2976.000242

$$A_1 = -\frac{R_{7AV}}{100R_{5AV}}x_4\left(x_3 - V_{1AV}\right)\left(x_3 - V_{2AV}\right) - \frac{R_{7AV}}{100R_{6AV}}x_3\left(x_3 + d_{AV}\right)\left(x_3 + e_{AV}\right) - \frac{R_{18AV}R_{7AV}}{R_{17AV}R_{9AV}}\left(\frac{R_{16AV}}{R_{14AV}}x_3 + \frac{R_{16AV}}{100R_{15AV}}x_3^3\right) + \frac{R_{7AV}}{R_{8AV}}\left[\frac{R_{11AV}R_{21AV}}{R_{20AV}}\left(\frac{R_{13AV}}{R_{12AV}+R_{13AV}}x_1 - \frac{1}{R_{10AV}}x_2\right) + \frac{R_{11AV}R_{21AV}}{100R_{19AV}}\left(\frac{R_{13AV}}{R_{12AV}+R_{13AV}}x_1 - \frac{1}{R_{10AV}}x_2\right)^3\right] \quad (51)$$

Starting from equation (50) and the SA oscillator equation (equation (1)), the relationships between the parameters are established by the correspondences given in equations (52), (53), and (54).

$$\frac{R_{7AV}}{100R_{5AV}} = \alpha_{AV}; C_{2AV}R_{2AV} = C_{1AV}R_{1AV} = 1 \text{ and } \frac{R_{7AV}}{100R_{6AV}} = \frac{1}{e_{AV}d_{AV}} \quad (52)$$

$$\frac{R_{18AV}R_{7AV}}{R_{17AV}R_{9AV}} = k_{SA-AV}; \frac{R_{16AV}}{R_{14AV}} = \frac{R_{16AV}}{100R_{15AV}} = 1; \frac{R_{7AV}}{R_{8AV}} = k_{SA-AV}^T \text{and} \frac{1}{R_{10AV}} = T_{SA-AV} \quad (53)$$

$$\frac{R_{11AV}R_{21AV}}{R_{20AV}} = 1; \frac{R_{13AV}}{R_{12AV}+R_{13AV}} = 1 \text{ and } \frac{R_{11AV}R_{21AV}}{100R_{19AV}} = 1 \quad (54)$$

Figure 19. Electronic equivalence of the circuit representing the HP oscillator mounted on OrCAD-PSpice software.

The analog equivalence for the HP oscillator is shown in Figure 18. This figure shows 21 resistors $\left(R_{1HP}, R_{2HP}, R_{3HP}, R_{4HP}, R_{5HP}, R_{6HP}, R_{7HP}, R_{8HP}, R_{9HP}, R_{10HP}, R_{11HP}, \ldots\ldots\ldots, \text{et } R_{21HP}\right)$, 2 capacitors $\left(C_{1HP} \text{ et } C_{2HP}\right)$, 8 operational amplifiers (TL082), 8 multipliers (AD633/AD), DC voltage sources to power integrated circuits (AOP and multipliers) for some, and for *o*thers they are used as equivalent circuit parameters.

Using Kirchhoff's laws, Ohm's law, and Taylor's series expansion, an analogous analysis to the AV oscillator is used to obtain the following relationships:

$$cc_2 = \frac{1}{10}\left(x_5 - V_{1HP}\right)\left(x_5 - V_{2HP}\right) \quad (55)$$

$$C_2 = \frac{1}{100}x_6\left(x_5 - V_{1HP}\right)\left(x_5 - V_{2HP}\right) \quad (56)$$

$$cc_3 = \frac{1}{10}\left(x_5 + d_{HP}\right)\left(x_5 + e_{HP}\right) \quad (57)$$

$$C_3 = \frac{1}{100}x_5\left(x_5 + d_{HP}\right)\left(x_5 + e_{HP}\right) \quad (58)$$

$$C_1 = C_{1HP}R_{1HP}\frac{dx_6}{dt} \text{ and } x_6 = C_{2HP}R_{2HP}\frac{dx_5}{dt} \quad (59)$$

$$C_7 = \frac{R_{11HP}R_{13HP}}{R_{12HP}+R_{13HP}}x_3 - \frac{R_{11HP}}{R_{10HP}}x_4 \quad (60)$$

$$C_8 = \frac{1}{100}\left(\frac{R_{11HP}R_{13HP}}{R_{12HP}+R_{13HP}}x_3 - \frac{R_{11HP}}{R_{10HP}}x_4\right)^3 \quad (61)$$

$$C_6 = \frac{1}{100}x_3^3 \quad (62)$$

Citation: Fonkou RF, Lima GS, Savi MA. On the Heart Rhythm Analysis by an Intelligent Control Method Using Artificial Neural Networks: Analytical Study and Electronic Simulation. J Cardiovasc Med Cardiol. 2026;13(3):42-72. Available from: https://dx.doi.org/10.17352/2455-2976.000242

$$C_5 = \frac{R_{18HP}R_{16HP}}{R_{17HP}R_{14HP}}x_5 + \frac{R_{18HP}R_{16HP}}{100R_{17HP}R_{15HP}}x_5^3 \tag{63}$$

$$C_4 = -\frac{R_{21HP}}{R_{20HP}}\left(\frac{R_{11HP}R_{13HP}}{R_{12HP}+R_{13HP}}x_3 - \frac{R_{11HP}}{R_{10HP}}x_4\right) - \frac{R_{21HP}}{100R_{19HP}}\left(\frac{R_{11HP}R_{13HP}}{R_{12HP}+R_{13HP}}x_3 - \frac{R_{11HP}}{R_{10HP}}x_4\right)^3 \tag{64}$$

$$C_1 = -\frac{R_{7HP}}{R_{5HP}}C_2 - \frac{R_{7HP}}{R_{6HP}}C_3 - \frac{R_{7HP}}{R_{9HP}}C_5 - \frac{R_{7HP}}{R_{8HP}}C_4 \tag{65}$$

The substitution in equation (65) of equations (56), (58), (63) and (64) gives the following equation (66).

$$C_1 = -\frac{R_{7HP}}{100R_{5HP}}x_6\left(x_5 - V_{1HP}\right)\left(x_5 - V_{2HP}\right) - \frac{R_{7HP}}{100R_{6HP}}x_5\left(x_5 + d_{HP}\right)\left(x_5 + e_{HP}\right) - \frac{R_{18HP}R_{7HP}}{R_{17HP}R_{9HP}}\left(\frac{R_{16HP}}{R_{14HP}}x_5 + \frac{R_{16HP}}{100R_{15HP}}x_5^3\right) + \frac{R_{7HP}}{R_{8HP}}\left[\frac{R_{11HP}R_{21HP}}{R_{20HP}}\left(\frac{R_{13HP}}{R_{12HP}+R_{13HP}}x_3 - \frac{1}{R_{10HP}}x_4\right) + \frac{R_{11HP}R_{21HP}}{100R_{19HP}}\left(\frac{R_{13HP}}{R_{12HP}+R_{13HP}}x_3 - \frac{1}{R_{10HP}}x_4\right)^3\right] \tag{66}$$

Equivalences between the parameters of the HP oscillator (equation (1)) and those of equation (66) are given by equations (67), (68) and (69).

$$\frac{R_{7HP}}{100R_{5HP}} = \alpha_{HP};\ C_{2HP}R_{2HP} = C_{1HP}R_{1HP} = 1 \text{ and } \frac{R_{7HP}}{100R_{6HP}} = \frac{1}{e_{HP}d_{HP}} \tag{67}$$

$$\frac{R_{18HP}R_{7HP}}{R_{17HP}R_{9HP}} = k_{AV-HP};\ \frac{R_{16HP}}{R_{14HP}} = \frac{R_{16HP}}{100R_{15HP}} = 1;\ \frac{R_{7HP}}{R_{8HP}} = k_{AV-HP}^{T} \text{ and } \frac{1}{R_{10HP}} = T_{AV-HP} \tag{68}$$

$$\frac{R_{11HP}R_{21HP}}{R_{20HP}} = 1,\ \frac{R_{13HP}}{R_{12HP}+R_{13HP}} = 1 \text{ and } \frac{R_{11HP}R_{21HP}}{100R_{19HP}} = 1 \tag{69}$$

The block wired in the OrCAD-PSpice software to generate the ECG signal is shown in figure (20).

Note that AOPs with single-input feedback capacitors can be described as integrator modules, and for multi-input cases, they are called integrator-summer modules. Note that these modules can be used to sum the system's monomials. The change from a negative to a positive sign is made using unity-gain inverter modules with a feedback resistor.

The values corresponding to each of the components used to generate the various signals are given in Table 3.

The curves presented are obtained for a simulation step size called maximum step size and given by Sc = 0.01s. The polarization

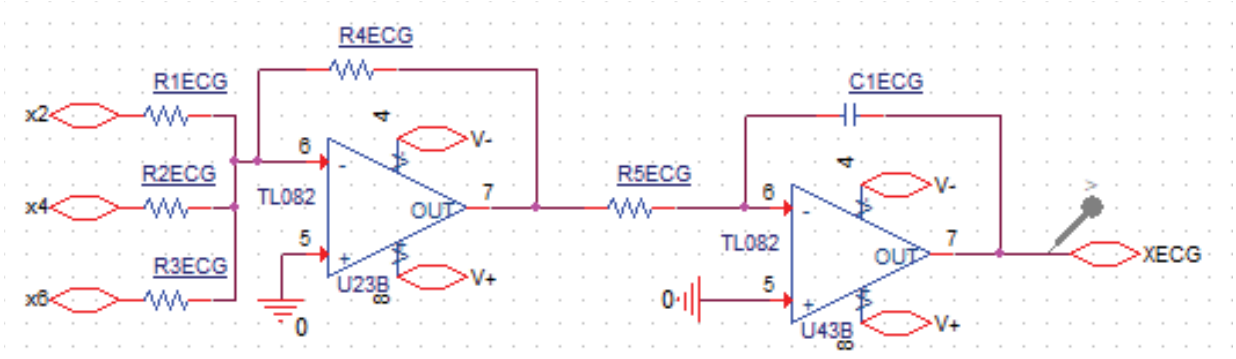

Figure 20: Electronic block for ECG signal generation mounted on OrCAD-PSpice software.

Citation: Fonkou RF, Lima GS, Savi MA. On the Heart Rhythm Analysis by an Intelligent Control Method Using Artificial Neural Networks: Analytical Study and Electronic Simulation. J Cardiovasc Med Cardiol. 2026;13(3):42-72. Available from: https://dx.doi.org/10.17352/2455-2976.000242

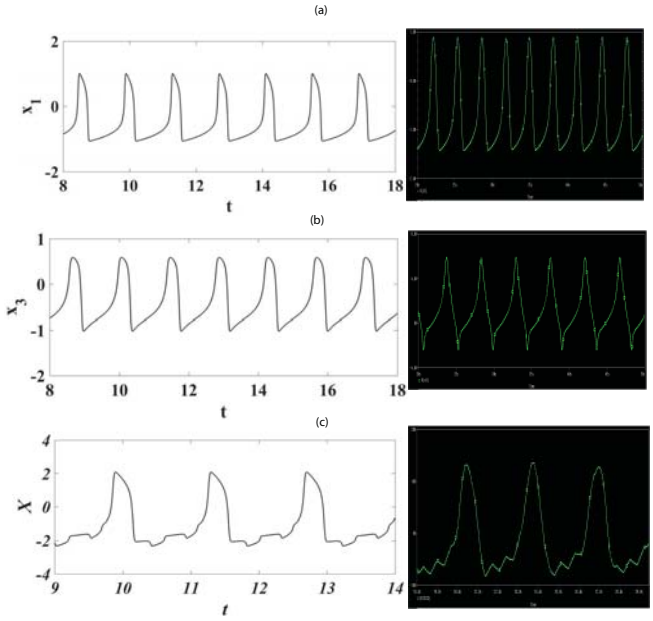

Figure 21: Curves obtained digitally and by electronic simulation with OrCAD-PSpice software: (a) case of SA oscillator; (b) case of AV oscillator; (c) case of ECG signal.

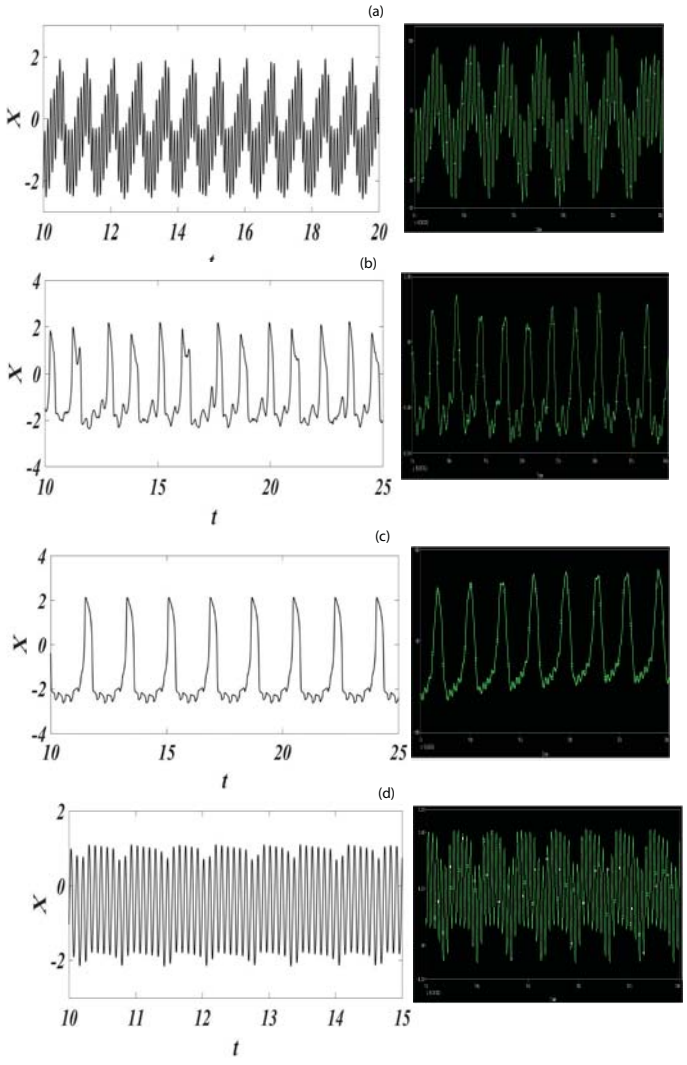

Figure 22: Synthetic ECGs obtained digitally and by electronic simulation with OrCAD-PSpice software: (a) ventricular fibrillation; (b) atrial fibrillation; (c) atrial flutter; (d) ventricular flutter.

Citation: Fonkou RF, Lima GS, Savi MA. On the Heart Rhythm Analysis by an Intelligent Control Method Using Artificial Neural Networks: Analytical Study and Electronic Simulation. J Cardiovasc Med Cardiol. 2026;13(3):42-72. Available from: https://dx.doi.org/10.17352/2455-2976.000242

Table 3: Values of the components used to obtain the normal ECG signal.

Oscillator type	Component values
Case of the SA oscillator	$R_{1SA} = 100\ k\Omega$; $C_{1SA} = 10\ \mu F$; $C_{2SA} = 100\ \mu F$; $R_{2SA} = 10\ k\Omega$ $R_{3SA} = 6\ k\Omega$; $R_{4SA} = 10\ k\Omega$; $R_{5SA} = 100\ \Omega$; $R_{6SA} = 250\ \Omega$ $R_{7SA} = 50\ M\Omega$ $V_{1SA} = 0.52\ V$; $V_{2SA} = -0.5\ V$; $d_{SA} = 2.0\ V$; $e_{SA} = 3.0\ V$
Case of the AV oscillator	$R_{1AV} = 5.5\ k\Omega$; $C_{1AV} = 100\ \mu F$; $C_{2AV} = 100\ \mu F$; $R_{2AV} = 10\ k\Omega$ $R_{3AV} = 2.5\ k\Omega$; $R_{4AV} = 700\ \Omega$; $R_{5AV} = 750\ \Omega$; $R_{6AV} = 50\ \Omega$ $R_{7AV} = 25\ M\Omega$; $R_{8AV} = 500\ \Omega$; $R_{9AV} = 750\ \Omega$; $R_{10AV} = 10\ k\Omega$ $R_{11AV} = 4\ k\Omega$; $R_{12AV} = 1\ k\Omega$; $R_{13AV} = 1\ k\Omega$; $R_{14AV} = 10\ k\Omega$ $R_{15AV} = 100\ \Omega$; $R_{16AV} = 10\ k\Omega$; $R_{17AV} = 8\ k\Omega$; $R_{18AV} = 1\ k\Omega$ $R_{19AV} = 200\ \Omega$; $R_{20AV} = 10\ k\Omega$; $R_{21AV} = 10\ k\Omega$ $V_{1AV} = 0.01\ V$; $V_{2AV} = -0.4\ V$; $d_{AV} = 3.0\ V$; $e_{AV} = 5.91\ V$
Case of the HP oscillator	$R_{1HP} = 1\ k\Omega$; $C_{1HP} = 100\ \mu F$; $C_{2HP} = 100\ \mu F$; $R_{2HP} = 10\ k\Omega$ $R_{3HP} = 5\ \Omega$; $R_{4HP} = 550\ \Omega$; $R_{5HP} = 2\ k\Omega$; $R_{6HP} = 5\ \Omega$ $R_{7HP} = 25\ M\Omega$; $R_{8HP} = 2\ k\Omega$; $R_{9HP} = 150\ \Omega$; $R_{10HP} = 10\ k\Omega$ $R_{11HP} = 4\ k\Omega$; $R_{12HP} = 1\ k\Omega$; $R_{13HP} = 250\ \Omega$; $R_{14HP} = 10\ k\Omega$ $R_{15HP} = 10\ \Omega$; $R_{16HP} = 10\ k\Omega$; $R_{17HP} = 1\ k\Omega$; $R_{18HP} = 4\ k\Omega$ $R_{19HP} = 10\ \Omega$; $R_{20HP} = 10\ k\Omega$; $R_{21HP} = 10\ k\Omega$ $V_{1HP} = 0.1\ V$; $V_{2HP} = -1.4\ V$; $d_{HP} = 7.0\ V$; $e_{HP} = 1.0\ V$
ECG Parameters	$R_{1ECG} = 7\ k\Omega$; $C_{1ECG} = 100\ \mu F$; $R_{2ECG} = 1\ M\Omega$; $R_{3ECG} = 66.67\ k\Omega$; $R_{4ECG} = 1.5\ k\Omega$; $R_{5ECG} = 500\ \Omega$

Table 4: Component values for the various pathologies

Diseases	Component values
Ventricular fibrillation	$R_{3HP} = 400\ \Omega$; $R_{5HP} = 2\ k\Omega$; $R_{1ECG} = 1\ M\Omega$; $R_{6HP} = 10\ k\Omega$ $R_{8SA} = 100\ k\Omega$; $R_{9SA} = 8\ \Omega$; $R_{2ECG} = 150\ k\Omega$; $R_{4ECG} = 10.5\ k\Omega$
Atrial fibrillation	$R_{9HP} = 5.15\ k\Omega$; $R_{3HP} = 300\ \Omega$; $R_{1ECG} = 16\ k\Omega$; $R_{6HP} = 100\ \Omega$ $R_{8SA} = 1\ M\Omega$; $R_{9SA} = 10\ \Omega$; $R_{2ECG} = 1\ M\Omega$; $R_{4ECG} = 1.5\ k\Omega$
Atrial flutter	$R_{3HP} = 400\ \Omega$; $R_{5HP} = 2\ k\Omega$; $R_{1ECG} = 12\ k\Omega$; $R_{6HP} = 10\ k\Omega$ $R_{8SA} = 3\ M\Omega$; $R_{9SA} = 10\ \Omega$;
Ventricular flutter	$R_{3HP} = 400\ \Omega$; $R_{5HP} = 2\ k\Omega$; $R_{1ECG} = 420\ k\Omega$; $R_{6HP} = 10\ k\Omega$ $R_{8SA} = 3\ M\Omega$; $R_{9SA} = 10\ \Omega$;

Citation: Fonkou RF, Lima GS, Savi MA. On the Heart Rhythm Analysis by an Intelligent Control Method Using Artificial Neural Networks: Analytical Study and Electronic Simulation. J Cardiovasc Med Cardiol. 2026;13(3):42-72. Available from: https://dx.doi.org/10.17352/2455-2976.000242

voltages V + and V – are 15 V and – 15 respectively.

Considering the normal case

$\left(F_{SA}(t) = \rho_{SA} \sin\left(\omega_{SA}(t)\right) = 0,\ F_{AV}(t) = \rho_{AV} \sin\left(\omega_{AV}(t)\right) = 0 \text{ and } F_{HP}(t) = \rho_{HP} \sin\left(\omega_{HP}(t)\right) = 0\right)$, Figure 21 compares some of the curves obtained by OrCAD-PSpice electronic simulation and digital simulation.

To obtain the diseased dynamics, the functional diagram given in figure 6 is considered. The curves obtained are shown in Figure 22. The basic values for obtaining the normal ECG given in Table 3 are maintained for some, and those modified according to the pathologies are given in Table 4. Note that the VSIN function represented by $f_{SA}(t)$ is parameterized according to the data specific to each disease (V_{AMPL} and FREQ).

Conclusion

In this work, it was a question of implementing a controller on an electronic system generating pathological heart rhythms. In order to bring pathological rhythms as close as possible to normal rhythms, an intelligent control system based on feedback linearization (FBL) was implemented, incorporating an artificial neural network to compensate for the unknown dynamics. The variable considered was the ECG signal. ECGs were generated using a reduced-order mathematical model consisting of three nonlinear oscillators linked by delayed Duffing-type connections incorporating cubic nonlinear terms. The dynamics produced showed close agreement with experimental measurements. The controller was applied to the SA node to track the trajectory of its signals so that it follows the desired state. The learning rate representing the incorporation of artificial neural networks into a Lyapunov-based control scheme was taken to be non-zero ($\mu \neq 0$), and adjusting the control parameter λ was used to improve the convergence of the closed-loop error. The results obtained show the effectiveness and robustness of the controller in avoiding the occurrence of a heart attack by approximating the ECG signal to the expected normal behavior. To demonstrate that the proposed heart model can derived from mathematical modeling, an electronic simulation using analog components has been carried out using OrCAD-Pspice software. The results obtained show good agreement with the numerical simulations.

Declarations

Funding statement: This research did not receive any specifi grant from funding agencies in the public, commercial, or not-for-profi sectors.

Data availability statement: No data was used for the research described in the article.

Declaration of interest_s statement: The authors declare no competing interests.

Additional information: No additional information is available for this paper.

(Appendix)

References

1. Nazari S, Heydari A, Khaligh J. Modified modeling of the heart by applying nonlinear oscillators and designing proper control signal. Appl Math. 2013;4(7):972-978. Available from: https://doi.org/10.4236/am.2013.47134

2. La Sala L, Crestani M, Garavelli S, de Candia P, Pontiroli AE. Does microRNA perturbation control the mechanisms linking obesity and diabetes? Implications for cardiovascular risk. Int J Mol Sci. 2021;22(1):143. Available from: https://doi.org/10.3390/ijms22010143

3. Fonkou RF, Kengne R, Fotsing Kamgang HC, Talla PK. Dynamical behavior analysis of the heart system by the bifurcation structures. Heliyon. 2023;9:e12887. Available from: https://doi.org/10.1016/j.heliyon.2023.e12887

4. Kuate GCG, Fotsin HB. On the nonlinear dynamics of a cardiac electrical conduction system model: theoretical and experimental study. Phys Scr. 2022;97:045205. Available from: https://doi.org/10.1088/1402-4896/ac5855

5. Savi MA. Chaos and order in biomedical rhythms. J Braz Soc Mech Sci Eng. 2005;27(2):157-169. Available from: https://doi.org/10.1590/S1678-58782005000200008

6. Kuate GCG, Mabekou Takam JS, Ngagoum FX, Fotsin HB. Multiple time-scales dynamics of a cardiac pacemaker model with application to heart rhythm modeling: theoretical study and FPGA implementation. Int J Bifurcat Chaos. 2022;32(7):2250106. Available from: https://doi.org/10.1142/S021812742250106

7. Britin SN, Britina MA, Vlasenko RY. Cardiac conduction system: a generalized electrical model. Biomed Eng. 2021;55:41-45. Available from: https://doi.org/10.1007/s10527-021-10067-1

Citation: Fonkou RF, Lima GS, Savi MA. On the Heart Rhythm Analysis by an Intelligent Control Method Using Artificial Neural Networks: Analytical Study and Electronic Simulation. J Cardiovasc Med Cardiol. 2026;13(3):42-72. Available from: https://dx.doi.org/10.17352/2455-2976.000242

8. van der Schouw YT, van der Graaf Y, Steyerberg EW, Eijkemans MJC, Banga JD. Age at menopause as a risk factor for cardiovascular mortality. Lancet. 1996;347:714-718. Available from: https://doi.org/10.1016/S0140-6736(96)90075-6

9. Venkat Narayan KM, Thompson TJ, Boyle JP, Beckles GLA, Engelgau MM, Vinicor F, et al. The use of population attributable risk to estimate the impact of prevention and early detection of type 2 diabetes on population-wide mortality risk in US males. Health Care Manag Sci. 1999;2:223-237. Available from: https://doi.org/10.1023/A:1019048114376

10. Cheffer A, Savi MA, Pereira TL, de Paula AS. Heart rhythm analysis using a nonlinear dynamics perspective. Appl Math Model. 2021;96:152-176. Available from: https://doi.org/10.1016/j.apm.2021.03.014

11. Cheffer A, Savi MA. Biochaos in cardiac rhythms. Eur Phys J Spec Top. 2022;231:833-845. Available from: https://doi.org/10.1140/epjs/s11734-021-00314-7

12. Fonkou RF, Kengne R, Wamba MD, Fotsing Kamgang HC, Talla PK. On the heart rhythm analysis using a nonlinear dynamics perspective: analytical study and electronic simulation. Phys Scr. 2024;99:055270. Available from: https://doi.org/10.1088/1402-4896/ad3d9c

13. Park DS, Fishman GI. The cardiac conduction system. Circulation. 2011;123(8):904-915. Available from: https://doi.org/10.1161/CIRCULATIONAHA.110.942284

14. Cheffer A, Ritto TG, Savi MA. Uncertainty analysis of heart dynamics using random matrix theory. Int J Non Linear Mech. 2021;129:103653. Available from: https://doi.org/10.1016/j.ijnonlinmec.2020.103653

15. Ryzhii E, Ryzhii M. Modeling of heartbeat dynamics with a system of coupled nonlinear oscillators. In: Proceedings of the International Conference on Biomedical Informatics and Technology. Berlin (Germany): Springer; 2013. p. 67-75. Available from: https://doi.org/10.1007/978-3-642-54121-6_6

16. Tung R, Boyle NG, Shivkumar K. Catheter ablation of ventricular tachycardia. Circulation. 2010;122:e389-e391. Available from: https://doi.org/10.1161/CIRCULATIONAHA.110.963371

17. Clyburn C, Sepe JJ, Habecker BA. What gets on the nerves of cardiac patients? Pathophysiological changes in cardiac innervation. J Physiol. 2022;600(3):451-461. Available from: https://doi.org/10.1113/JP281118

18. Yokokawa M, Kim HM, Good E, Crawford T, Chugh A, Pelosi F Jr, et al. Impact of QRS duration of frequent premature ventricular complexes on the development of cardiomyopathy. Heart Rhythm. 2012;9:1460-1464. Available from: https://doi.org/:10.1016/j.hrthm.2012.04.036

19. Viskin S, Ish-Shalom M, Koifman E, Rozovski U, Zeltser D, Glick A, et al. Ventricular flutter induced during electrophysiologic studies in patients with old myocardial infarction: clinical and electrophysiologic predictors, and prognostic significance. J Cardiovasc Electrophysiol. 2003;14(9):913-919. Available from: https://doi.org/10.1046/j.1540-8167.2003.03082.x

20. Loen V, Vos AM, van der Heyden M. The canine chronic atrioventricular block model in cardiovascular preclinical drug research. Br J Pharmacol. 2022;179:859-881. Available from: https://doi.org/10.1111/bph.15436

21. Kashou HA, Adedinsewo AD, Peter A. Subclinical atrial fibrillation: a silent threat with uncertain implications. Annu Rev Med. 2022;73:355-362. Available from: https://doi.org/10.1146/annurev-med-042420-105906

22. Van der Pol B, Van der Mark J. The heartbeat as a negative resistance oscillator, and an electrical model of the heart. Philos Mag. 1928;6(38):763-775. Available from: https://doi.org/10.1080/1478644110856465 .

23. Fonkou RF, Louodop P, Talla PK, Woafo P. Van der Pol equation with sinusoidal nonlinearity: dynamic behaviour and real-time control of a target trajectory. Phys Scr. 2021;96:125203. Available from: https://doi.org/10.1088/1402-4896/ac19cd

24. Fonkou RF, Louodop P, Talla PK, Woafo P. Dynamic behaviour of pacemaker models subjected to a blood pressure excitation simulator: a theoretical and experimental study by microcontroller. Braz J Phys. 2021;51:1448-1458. Available from: https://doi.org/10.1007/s13538-021-00967-8

25. Fonkou RF, Louodop P, Talla PK. Nonlinear oscillators with variable state damping and elastic coefficients. Pramana J Phys. 2021;95:210. Available from: https://doi.org/10.1007/s12043-021-02230-w

26. Fonkou RF, Louodop P, Talla PK, Woafo P. Analysis of the dynamics of new models of nonlinear systems with state variable damping and elastic coefficients. Heliyon. 2022;8:e10112. Available from: https://doi.org/10.1016/j.heliyon.2022.e10112

27. Fonkou RF, Kengne R, Fotsing Kamgang HC, Talla PK. Dynamical behavior analysis of the Van der Pol oscillator with sine nonlinearity subjected to non-sinusoidal periodic excitations by the bifurcation structures. Phys Scr. 2023;98:085014. Available from: https://doi.org/10.1088/1402-4896/ace8cf

28. FitzHugh R. Impulses and physiological states in theoretical models of nerve membrane. Biophys J. 1961;1:445-466. Available from: https://doi.org/10.1016/S0006-3495(61)86902-6

29. Hodgkin AL, Huxley AF. A quantitative description of membrane current and its applications to conduction and excitation in nerve. J Physiol. 1952;117:500-544. Available from: https://doi.org/10.1113/jphysiol.1952.sp004764

30. Gois RFSM, Savi MA. An analysis of heart rhythm dynamics using a three-coupled oscillator model. Chaos Solitons Fractals. 2009;41:2553-2565. Available from: https://doi.org/10.1016/j.chaos.2008.09.040

31. Fonkou RF, Louodop P, Talla PK. Dynamic behaviour of the cardiac conduction system under external disturbances: simulation based on microcontroller technology. Phys Scr. 2022;97:025001. Available from: https://doi.org/10.1088/1402-4896/ac47ba

Citation: Fonkou RF, Lima GS, Savi MA. On the Heart Rhythm Analysis by an Intelligent Control Method Using Artificial Neural Networks: Analytical Study and Electronic Simulation. J Cardiovasc Med Cardiol. 2026;13(3):42-72. Available from: https://dx.doi.org/10.17352/2455-2976.000242

32. De Paula AS, Savi MA, Wiercigroch M, Pavlovskaia E. Bifurcation control of a parametric pendulum. Int J Bifurcat Chaos. 2012;22(5):1250111. Available from: https://doi.org/10.1142/S0218127412501118

33. Elayan H, Aloqaily M, Guizani M. Digital twin for intelligent context-aware IoT healthcare systems. IEEE Internet Things J. 2021;8(23):16749-16757. Available from: https://doi.org/10.1109/JIOT.2021.3051158

34. Surucu M, Isler Y, Perc M, Kara R. Convolutional neural networks predict the onset of paroxysmal atrial fibrillation: theory and applications. Chaos. 2021;31(11):113119. Available from: https://doi.org/10.1063/5.0069272

35. Wang R, Fan J, Li Y. Deep multi-scale fusion neural network for multi-class arrhythmia detection. IEEE J Biomed Health Inform. 2020;24(9):2461-2472. Available from: https://doi.org/10.1109/JBHI.2020.2981526

36. Fonkou RF, Savi MA. Heart rhythm analysis using nonlinear oscillators with Duffing-type connections. Fractal Fract. 2023;7:592. Available from: https://doi.org/10.3390/fractalfract7080592

37. Krstacic G, Krstacic A, Smalcelj A, Milicic D, Jembrek-Gostovic M. The chaos theory and nonlinear dynamics in heart rate variability analysis: does it work in short-time series in patients with coronary heart disease? Ann Noninvasive Electrocardiol. 2007;12:130-136. Available from: https://doi.org/10.1111/j.1542-474X.2007.00151.x

38. Ernst J, Bar-Joseph Z. STEM: a tool for the analysis of short time series gene expression data. BMC Bioinformatics. 2006;7:191. Available from: https://doi.org/10.1186/1471-2105-7-191

39. Tobón DP, Jayaraman S, Falk TH. Spectro-temporal electrocardiogram analysis for noise-robust heart rate and heart rate variability measurement. IEEE J Transl Eng Health Med. 2017;5:1-11. Available from: https://doi.org/10.1109/JTEHM.2017.27676

40. Mulpuru SK, Madhavan M, McLeod CJ, Cha YM, Friedman PA. Cardiac pacemakers: function, troubleshooting, and management. J Am Coll Cardiol. 2017;69(2):189-210. Available from: https://doi.org/10.1016/j.jacc.2016.10.061

41. Lima GS, Savi MA, Bessa WM. Intelligent control of cardiac rhythms using artificial neural networks. Nonlinear Dyn. 2023;111:11543-11557. Available from: https://doi.org/10.1007/s11071-023-08447-1

42. Garfinkel A, Weiss JN, Ditto WL, Spano ML. Chaos control of cardiac arrhythmias. Trends Cardiovasc Med. 1995;5(2):76-80. Available from: https://doi.org/10.1016/1050-1738(94)00083-2

43. Karar ME. Robust RBF neural network-based backstepping controller for implantable cardiac pacemakers. Int J Adapt Control Signal Process. 2018;32(7):1040-1051. Available from: https://doi.org/10.1002/acs.2884

44. Lounis F, Boukabou A, Soukkou A. Implementing high-order chaos control scheme for cardiac conduction model with pathological rhythms. Chaos Solitons Fractals. 2020;132:109581. Available from: https://doi.org/10.1016/j.chaos.2019.109581

45. Garfinkel A, Spano ML, Ditto WL, Weiss JN. Controlling cardiac chaos. Science. 1992;257(5074):1230-1235. Available from: https://doi.org/10.1126/science.1519060

46. Ferreira BB, De Paula AS, Savi MA. Chaos control applied to heart rhythm dynamics. Chaos Solitons Fractals. 2011;44(8):587-599. Available from: https://doi.org/10.1016/j.chaos.2011.05.009

47. Ferreira BB, Savi MA, De Paula AS. Chaos control applied to cardiac rhythms represented by ECG signals. Phys Scr. 2014;89(10):105203. Available from: https://doi.org/10.1088/0031-8949/89/10/105203

48. Quiroz-Juárez M, Jiménez-Ramírez O, Vázquez-Medina R, Breña-Medina V, Aragón JL, Barrio RA. Generation of ECG signals from a reaction-diffusion model spatially discretized. Sci Rep. 2019;9(1):1-10. Available from: https://doi.org/10.1038/s41598-019-55448-5

49. Khan A, Nigar U. Combination projective synchronization in fractional-order chaotic system with disturbance and uncertainty. Int J Appl Comput Math. 2020;6(4):1-22. Available from: https://doi.org/10.1007/s40819-020-00852-z

50. Gharesi N, Arefi MM, Khayatian A, Bahrami Z. Extended state observer-based control of heartbeat described by heterogeneous coupled oscillator model. Commun Nonlinear Sci Numer Simul. 2021;101:105884. Available from: https://doi.org/10.1016/j.cnsns.2021.105884

51. Elayan H, Aloqaily M, Guizani M. Digital twin for intelligent context-aware IoT healthcare systems. IEEE Internet Things J. 2021;8(23):16749-16757. Available from: https://doi.org/10.1109/JIOT.2021.3051158

52. Surucu M, Isler Y, Perc M, Kara R. Convolutional neural networks predict the onset of paroxysmal atrial fibrillation: theory and applications. Chaos. 2021;31(11):113119. Available from: https://doi.org/10.1063/5.0069272

53. Wang R, Fan J, Li Y. Deep multi-scale fusion neural network for multi-class arrhythmia detection. IEEE J Biomed Health Inform. 2020;24(9):2461-2472. Available from: https://doi.org/10.1109/JBHI.2020.2981526

54. Bessa WM, Brinkmann G, Duecker DA, Kreuzer E, Solowjow E. A biologically inspired framework for the intelligent control of mechatronic systems and its application to a micro diving agent. Math Probl Eng. 2018;2018:9648126. Available from: https://doi.org/10.1155/2018/9648126

55. Dos Santos JDB, Bessa WM. Intelligent control for accurate position tracking of electrohydraulic actuators. Electron Lett. 2019;55(2):78-80. Available from: https://doi.org/10.1049/el.2018.7218

Citation: Fonkou RF, Lima GS, Savi MA. On the Heart Rhythm Analysis by an Intelligent Control Method Using Artificial Neural Networks: Analytical Study and Electronic Simulation. J Cardiovasc Med Cardiol. 2026;13(3):42-72. Available from: https://dx.doi.org/10.17352/2455-2976.000242

56. Lima GS, Porto DR, de Oliveira AJ, Bessa WM. Intelligent control of a single-link flexible manipulator using sliding modes and artificial neural networks. Electron Lett. 2021;57(23):869-872. Available from: https://doi.org/10.1049/ell2.12300

57. Karar ME. Robust RBF neural network-based backstepping controller for implantable cardiac pacemakers. Int J Adapt Control Signal Process. 2018;32(7):1040-1051. Available from: https://doi.org/10.1002/acs.2884

58. Irisawa H, Brown HF, Giles W. Cardiac pacemaking in the sinoatrial node. Physiol Rev. 1993;73(1):197-227. Available from: https://doi.org/10.1152/physrev.1993.73.1.197

59. Anderson RH, Yanni J, Boyett MR, Chandler NJ, Dobrzynski H. The anatomy of the cardiac conduction system. Clin Anat. 2009;22(1):99-113. Available from: https://doi.org/10.1002/ca.20681

60. Severs NJ, Bruce AF, Dupont E, Rothery S. Remodelling of gap junctions and connexin expression in diseased myocardium. Cardiovasc Res. 2008;80(1):9-19. Available from: https://doi.org/10.1093/cvr/cvn133

61. Kleber AG, Rudy Y. Basic mechanisms of cardiac impulse propagation and associated arrhythmias. Physiol Rev. 2004;84(2):431-488. Available from: https://doi.org/10.1152/physrev.00025.2003

62. Grudzinski K, Zebrowski JJ. Modeling cardiac pacemakers with relaxation oscillators. Physica A. 2004;336:153-162. Available from: https://doi.org/10.1016/j.physa.2004.01.020

63. Cunningham WJ. A nonlinear differential-difference equation of growth. Proc Natl Acad Sci U S A. 1954;40(8):708-713. Available from: https://doi.org/10.1073/pnas.40.8.708

64. Zheng Z, Lin J, Hu Y, Zhou Q, Yi C. Dynamic unbalance identification and quantitative diagnosis of cardan shaft in high-speed train based on improved TQWT-RBFNN-NSGA-II method. Eng Fail Anal. 2022;136:106226. Available from: https://doi.org/10.1016/j.engfailanal.2022.106226

65. World Health Organization. Cardiovascular diseases (CVDs) [Internet]. Geneva: World Health Organization; 2020 [cited 2020 Dec 13]. Available from: https://www.who.int/news-room/fact-sheets/detail/cardiovascular-diseases-(cvds)

66. Kim YG, Choi YY, Han KD, Min K, Choi HY, Shim J, et al. Atrial fibrillation is associated with increased risk of lethal ventricular arrhythmias. Sci Rep. 2021;11:18111. Available from: https://doi.org/10.1038/s41598-021-97335-y

67. PhysioNet. PhysioNet Databases [Internet]. Cambridge (MA): PhysioNet; 2020 [cited 2020 Dec 10]. Available from: https://physionet.org/about/database/

68. Davies MJ, Pomerance A. Pathology of atrial fibrillation in man. Br Heart J. 1972;34(5):520-525. Available from: https://doi.org/10.1136/hrt.34.5.520

69. Diamant MJ, Andrade JG, Virani SA, Jhund PS, Petrie MC, Hawkins NM. Heart failure and atrial flutter: a systematic review of current knowledge and practices. ESC Heart Fail. 2021;8:4484-4496. Available from: https://doi.org/10.1002/ehf2.13526

70. Wiggers CJ. The mechanism and nature of ventricular fibrillation. Am Heart J. 1940;20(4):399-412. Available from: https://doi.org/10.1016/S0002-8703(40)90874-2

71. Bessa WM, De Paula AS, Savi MA. Sliding mode control with adaptive fuzzy dead-zone compensation for uncertain chaotic systems. Nonlinear Dyn. 2012;70(3):1989-2001. Available from: https://doi.org/10.1007/s11071-012-0591-z

72. Bessa WM, De Paula AS, Savi MA. Adaptive fuzzy sliding mode control of a chaotic pendulum with noisy signals. Z Angew Math Mech. 2014;94(3):256-263. Available from: https://doi.org/10.1002/zamm.201200214

73. Bessa WM, Kreuzer E, Lange J, Pick MA, Solowjow E. Design and adaptive depth control of a micro diving agent. IEEE Robot Autom Lett. 2017;2(4):1871-1877. Available from: https://doi.org/10.1109/LRA.2017.2714142

74. Bessa WM, Otto S, Kreuzer E, Seifried R. An adaptive fuzzy sliding mode controller for uncertain underactuated mechanical systems. J Vib Control. 2019;25(9):1521-1535. Available from: https://doi.org/10.1177/1077546319827393

75. Bessa WM, De Paula AS, Savi MA. Adaptive fuzzy sliding mode control of smart structures. Eur Phys J Spec Top. 2013;222(7):1541-1551. Available from: https://doi.org/10.1140/epjst/e2013-01943-7

76. Park J, Sandberg IW. Universal approximation using radial-basis-function networks. Neural Comput. 1991;3(2):246-257. Available from: https://doi.org/10.1162/neco.1991.3.2.246

77. Ioannou P, Fidan B. Adaptive Control Tutorial. Philadelphia (PA): Society for Industrial and Applied Mathematics (SIAM); 2006. Available from: https://books.google.co.in/books/about/Adaptive_Control_Tutorial.html?id=o7d0R6Zj2pMC&redir_esc=yences

Citation: Fonkou RF, Lima GS, Savi MA. On the Heart Rhythm Analysis by an Intelligent Control Method Using Artificial Neural Networks: Analytical Study and Electronic Simulation. J Cardiovasc Med Cardiol. 2026;13(3):42-72. Available from: https://dx.doi.org/10.17352/2455-2976.000242